JOURNAL OF GEOPHYSICAL RESEARCH, VOL. 105, NO. B3, PAGES 5835–5857, MARCH 10, 2000

Geophysical evidence for the evolution of the California Inner Continental Borderland as a metamorphic core complex

Uri S. ten Brink,[1] Jie Zhang,[2,3] Thomas M. Brocher,[4] David A. Okaya,[5] Kim D. Klitgord,[4,6] and Gary S. Fuis[4]

Abstract. We use new seismic and gravity data collected during the 1994 Los Angeles Region Seismic Experiment (LARSE) to discuss the origin of the California Inner Continental Borderland (ICB) as an extended terrain possibly in a metamorphic core complex mode. The data provide detailed crustal structure of the Borderland and its transition to mainland southern California. Using tomographic inversion as well as traditional forward ray tracing to model the wide-angle seismic data, we find little or no sediments, low (≤6.6 km/s) *P* wave velocity extending down to the crust-mantle boundary, and a thin crust (19 to 23 km thick). Coincident multichannel seismic reflection data show a reflective lower crust under Catalina Ridge. Contrary to other parts of coastal California, we do not find evidence for an underplated fossil oceanic layer at the base of the crust. Coincident gravity data suggest an abrupt increase in crustal thickness under the shelf edge, which represents the transition to the western Transverse Ranges. On the shelf the Palos Verdes Fault merges downward into a landward dipping surface which separates "basement" from low-velocity sediments, but interpretation of this surface as a detachment fault is inconclusive. The seismic velocity structure is interpreted to represent Catalina Schist rocks extending from top to bottom of the crust. This interpretation is compatible with a model for the origin of the ICB as an autochthonous formerly hot highly extended region that was filled with the exhumed metamorphic rocks. The basin and ridge topography and the protracted volcanism probably represent continued extension as a wide rift until ~13 m.y. ago. Subduction of the young and hot Monterey and Arguello microplates under the Continental Borderland, followed by rotation and translation of the western Transverse Ranges, may have provided the necessary thermomechanical conditions for this extension and crustal inflow.

1. Introduction

Continental extension is a ubiquitous process and is manifested by a diversity of basin architecture and magmatic construction. This diversity is due to lithospheric conditions prior to and during extension [e.g., *Buck*, 1991], but these conditions are often poorly known. Lithospheric conditions of the California Inner Continental Borderland (ICB) offshore southern California prior to the rifting can be deduced with some confidence because the ICB is located in the forearc region of a long-lived subduction zone where subduction ceased shortly before extension took place [*Atwater*, 1989]. The ICB is surrounded by the forearc lithotectonic provinces of the western Transverse Range (WTR) and the California Outer Continental Borderland (OCB), the accreted arcs and melanges of the Western Foothills belt, and the magmatic arc of the Peninsular Ranges (Figure 1). Although its submerged basin and ridge area is physiographically similar to the OCB (Figure 2), its composition is different from the other forearc provinces. The exposed and drilled basement of the ICB is the medium to high-grade metamorphic rocks, known as the Catalina Schist, which were brought to the surface from 10–15 km depths during the Middle Miocene [e.g., *Crouch and Suppe*, 1993]. The ICB is bounded by the Eastern Santa Cruz Basin Fault to the west, the Santa Monica–Dume Fault zone to the north, and the Newport-Inglewood Fault zone to the east (Figures 1 and 2; *Vedder* [1987]). Voluminous Miocene volcanic rocks line the boundaries of the ICB and outcrop within it [*Hurst*, 1982; *Weigand and Savage*, 1993; *Dickinson*, 1997]. The emplacement of the schist was, according to *Crouch and Suppe* [1993], the result of extreme crustal extension and exhumation in the form of a metamorphic core complex. Other models, however, suggested that the Catalina Schist was emplaced by a northward translation of an "exotic terrain" along strike-slip faults [e.g., *Vedder*, 1987]. Others explained the exposures of high-pressure metamorphic rocks by recent transpressional motion that brought slivers of material up from the lower crust [*Mann and Gordon*, 1996].

A corollary issue to the legacy of subduction is whether or not a subducted slab is present under the ICB. Seismic data across the California continental margin to the north [*Crandall et al.*, 1983; *Miller et al.*, 1992; *Brocher et al.*, 1999] suggested the existence of an underlying fossil ocean crust between the former trench and the San Andreas Fault. A landward dipping top of the oceanic crust can be imaged for only a few kilome-

[1]U.S. Geological Survey, Woods Hole, Massachusetts.
[2]Earth Resources Laboratory, Massachusetts Institute of Technology, Cambridge.
[3]Now at Geotomo Ltd., Louisville, Colorado.
[4]U.S. Geological Survey, Menlo Park, California.
[5]Department of Geological Sciences, University of Southern California, Los Angeles.
[6]Now at Exxon Exploration Company, Houston, Texas.

Paper number 1999JB900318.
0148-0227/00/1999JB900318$09.00

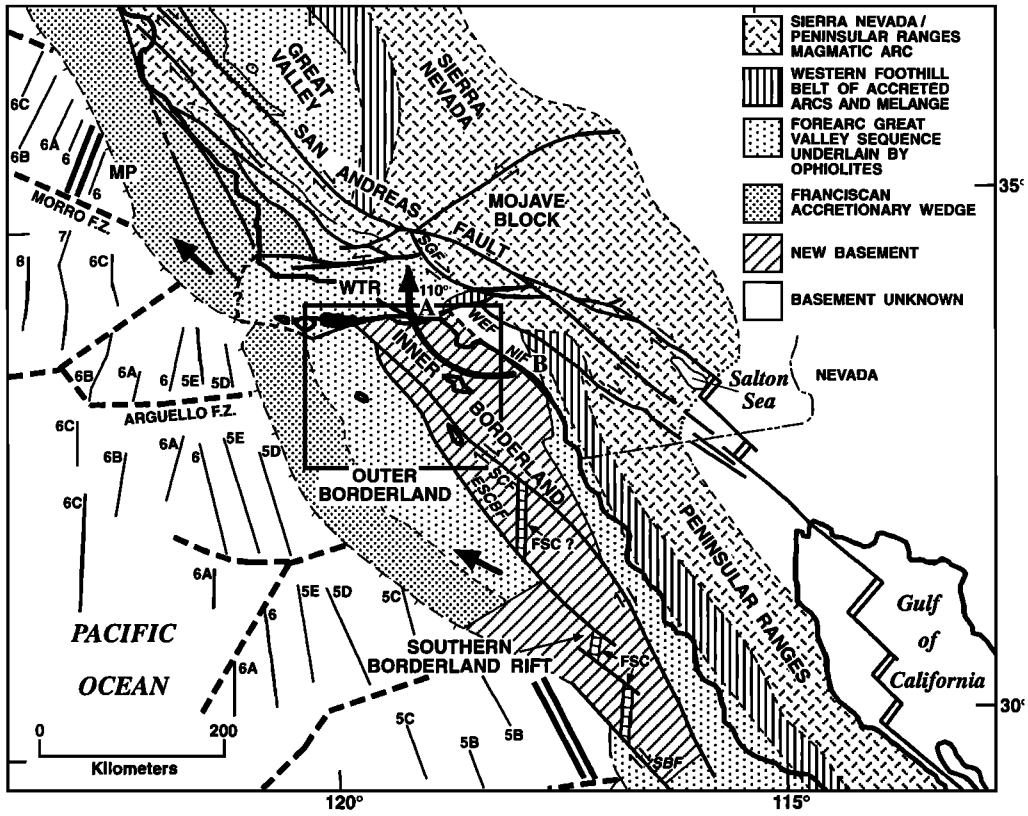

Figure 1. Principal lithotectonic belts in southern California and offshore magnetic anomalies (modified from *Crouch and Suppe* [1993], *Wright* [1991], and *Atwater and Severinghaus* [1989]). Rectangle shows location of Figure 2. Arrows show northwestward translation of the California Outer Continental Borderland and 110° rotation and translation of the Transverse Ranges. ESCBF, Eastern Santa Cruz Basin Fault; FSC, Fossil spreading center; MP, Monterey microplate; NIF, Newport-Inglewood Fault; SBF, San Benito Fault; SCF, San Clemente Fault; SGF, San Gabriel Fault; WEF, Whittier-Elsinore Fault; WTR, western Transverse Ranges. A and B, locations of Santa Monica Mountains–Simi Hills and of San Joaqin Hills, respectively.

ters east of the ocean-continent boundary of the California Borderland, but gravity data have been used to suggest that this layer extends eastward to shore [*Miller et al.*, 1996]. *Dickinson* [1997], on the other hand, suggested that the oceanic slab underlying the ICB foundered during the Middle Miocene, giving rise to volcanism.

Despite the ICB's proximity to the Los Angeles metropolitan area, surprisingly little work has been focused on its deeper structure. Most of the evidence contributing to these debates has been from rock outcrops, dredges, oil exploration wells, and seismic reflection data in the upper few kilometers of the sediments and crust [e.g., *Crouch and Suppe*, 1993; *Bohannon and Geist*, 1998]. Crustal seismic refraction work was carried out in the ICB between 1948 and 1955 [*Shor and Raitt*, 1958], and multichannel seismic (MCS) reflection techniques have proven ineffective in imaging the lower crust and the Moho there. Crustal tomographic studies using earthquake sources in southern California [e.g., *Hearn and Clayton*, 1986; *Sung and Jackson*, 1992; *Hauksson and Haase*, 1997] poorly constrained crustal structure within the ICB because of sparse ray coverage.

The offshore component of the Los Angeles Region Seismic Experiment (LARSE) project, conducted during October 1994, was designed to map in detail the crustal structure of the ICB and its transition to mainland California. We report here the analysis and interpretation of coincident wide-angle seismic reflection and refraction data, multichannel seismic (MCS) reflection data, and gravity data recorded as part of LARSE along two lines crossing the ICB (Figure 2). We then discuss the implications of our crustal velocity structure to the past tectonic history of the region and, in particular, to the origin of the ICB as a metamorphic core complex.

2. Tectonic Overview

Subduction of the Farallon Plate beneath North America during the Mesozoic and Paleogene formed the arc-trench system which includes the Franciscan accretionary wedge, the Great Valley forearc-basin sequence and the underlying Coast Range ophiolites, the accreted arcs and melanges of the Western Foothills belt, and the magmatic arc of the Sierra Nevada-Peninsular Ranges (Figure 1; *Crouch and Suppe* [1993]). This arc-trench system was disrupted following the first encounter of the East Pacific Rise with North America at ~28 Ma, which probably occurred at the latitude of the California Borderland [*Atwater and Stock*, 1998]. The Monterey microplate fragment of the Farallon Plate stopped subducting under central California at 20–18 Ma, and the Arguello microplate immediately to the south continued subducting until ~17.5 Ma [*Nicholson et al.*, 1994]. To account for seismic observations favoring a remnant slab of oceanic crust beneath the margin in central California [*Miller et al.*, 1992], *Nicholson et al.* [1994] proposed

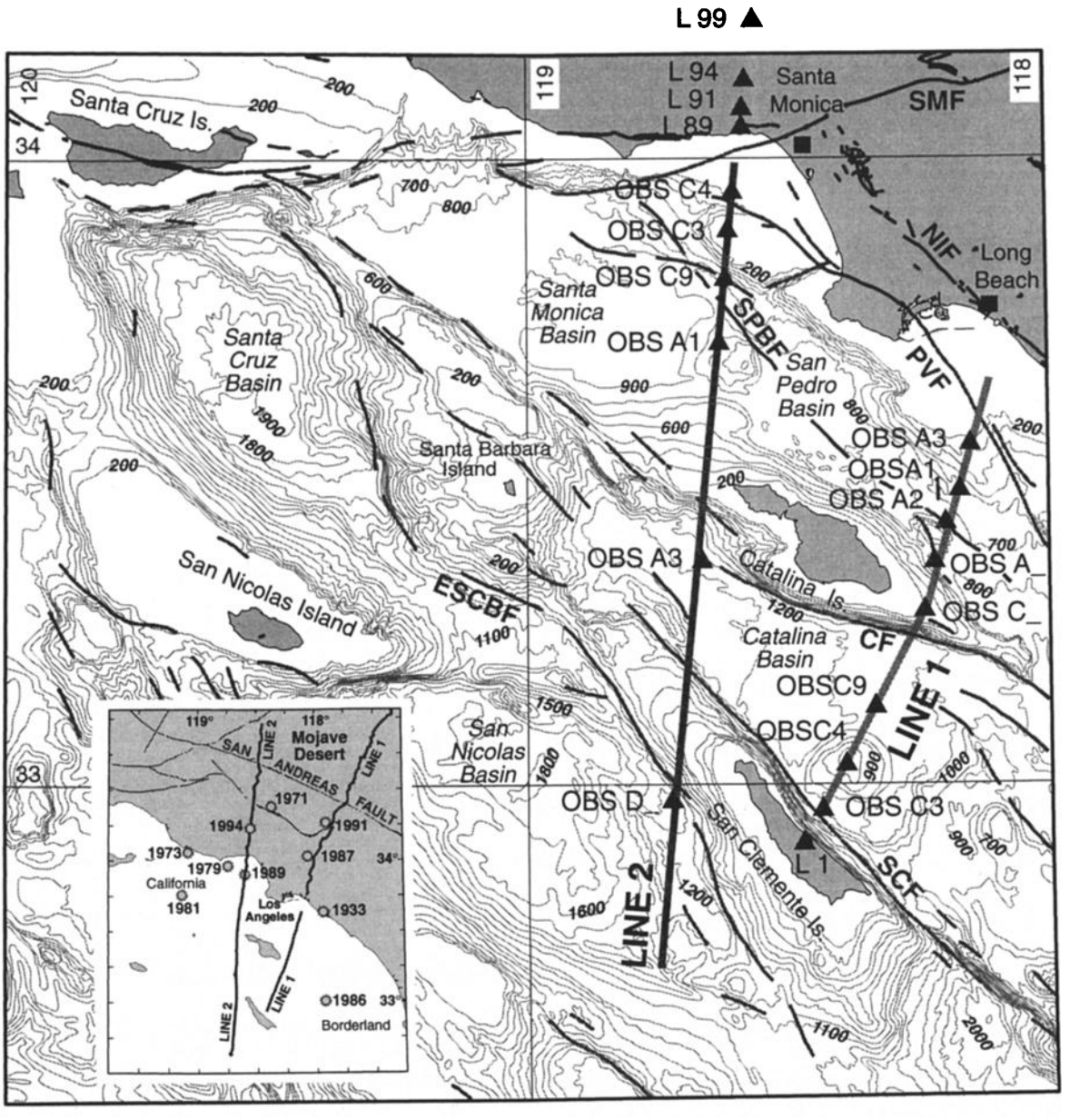

Figure 2. Bathymetry of the California Inner Continental Borderland (ICB) (contour interval 100 m), location of air gun shots along lines 1 and 2 (thick lines), ocean bottom seismometer locations and land stations used in this study (triangles), and major faults (thin lines). Inset shows location of onshore-offshore Los Angeles Region Seismic Experiment (LARSE) lines 1 and 2 and location of major earthquakes (circles annotated by year). Fault abbreviations are as follows: Catalina (CF), East Santa Cruz Basin (ESCBF), Newport-Inglewood (NIF), Palos Verde (PVF), San Clemente (SCF), Santa Monica (SMF), and San Pedro Basin (SPBF).

that subducted Monterey microplate there exists under the margin eastward to the San Andreas Fault. They further proposed that the partially subducted Monterey microplate under the WTR was captured by the Pacific Plate when the Pacific–North American Plate boundary jumped inboard of the WTR. As the Pacific Plate continued to move northward relative to North America, it attempted to drag the WTR with it. However, because of the jog in the plate boundary the WTR rotated (Figure 3; *Nicholson et al.* [1994]). We suggest that the underlying Monterey microplate was torn as a result of this rotation, with part of the Monterey microplate being rotated and translated with the WTR while the inboard part remained in place. Asthenospheric upper mantle may have filled the gap in the wake of this tear (Figure 3).

The western Transverse Ranges were rotated ~110° clockwise during the last 20–18 Myr [*Luyendyk*, 1991], becoming perpendicular to the margin (Figure 1). *Crouch and Suppe* [1993] proposed that the ICB, including the area now occupied by the Los Angeles Basin, was extended in the wake of this rotation producing metamorphic core complexes and shallow detachments faults. According to their model the Catalina Schist is part of the Franciscan belt which has been exhumed in situ from midcrustal levels (10–15 km). The Catalina Schist represents a footwall metamorphic tectonite, which has been

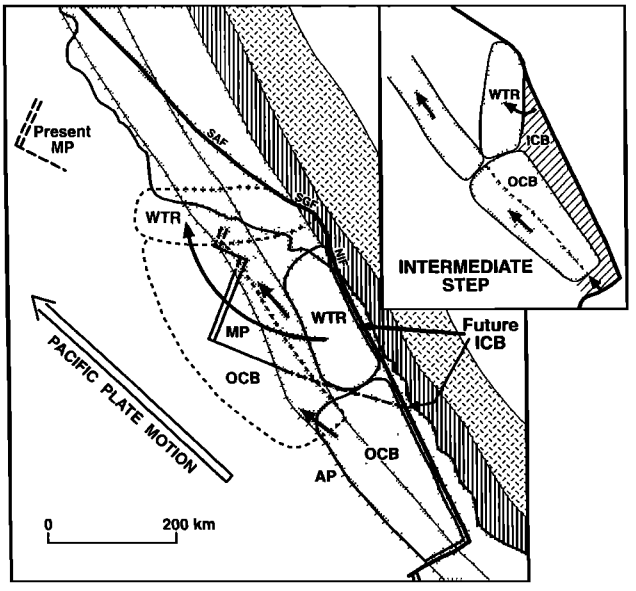

Figure 3. Relative positions of the lithostatic units of the California margin prior to the tectonic evolution of the ICB. Original locations of the western Transverse Ranges (WTR) and the California Outer Continental Borderland (OCB) are marked by thin lines [after *Nicholson et al.*, 1994], and their present locations are marked by dashed lines. Heavy line, plate boundary when the ICB was extended. Open arrow, magnitude and general direction of Pacific Plate motion relative to North America based on the present location of the remnant Monterey microplate (MP) 20 Myr ago. Additional bulk translation of the entire margin by several hundreds of kilometers since the Miocene [e.g., *Nicholson et al.*, 1994] is omitted to help focus on the internal rotations and translations within the margin. When the MP ceased subducting under the California margin 18–20 Myr ago, it was captured and dragged by the northwestward moving Pacific Plate [*Nicholson et al.*, 1994]. The overlying WTR was dragged with it but rotated because a bend in the newly formed plate boundary limited its northward migration. The stalled MP possibly tore as the WTR rotated, allowing for localized short-lived mantle upwelling. About 1(?) m.y. later, the Arguello microplate (AP) south of the MP ceased subducting and was captured by the Pacific Plate, dragging the overriding OCB northwestward with it [*Nicholson et al.*, 1994]. As a result, the new plate boundary propagated southward, and the ICB expanded to the south as shown here.

tectonically denuded and partially eroded. The hanging wall (or upper plate) rocks are formed by the Great Valley forearc sequence and its underlying basement, and they now comprise the rotated Santa Monica Mountains and Simi Hills to the north and the unrotated San Joaquin Hills to the east (A and B, respectively, in Figure 1). Part of the detachment separating the "upper" and "lower" plates is proposed to be dipping landward from the eastern edge of the ICB, and the Newport-Inglewood and Whittier-Elsinore Faults are proposed to have been originally high-angle normal faults that terminated against this major detachment. The total extension in the ~100-km-wide ICB is estimated at between 200–250 km [*Crouch and Suppe*, 1993] and 100 km [*Atwater and Stock*, 1998; *Bohannon and Geist*, 1998].

In addition to rotation and extension the ICB served as the location of the Pacific-North American transform plate boundary until ~12 Ma (Figures 1 and 3). The area connected the ancestral San Andreas Fault east of the Transverse Ranges with the San Benito Fault on the western continental margin of Baja California [*Nicholson et al.*, 1994; *Ingersoll and Rumelhart*, 1999]. The capture of Arguello microplate by the Pacific Plate caused the California Outer Continental Borderland (OCB) to move northwestward relative to North America along this plate boundary (Figure 3). Extension in the Gulf of California started at 12–14 Ma, and the plate boundary finally jumped to the Gulf of California at 5–6 Ma. As a result of this jump, most of the relative plate motion in southern California is now accommodated inland of the coast, with only up to 14% (~7 mm/yr) being accommodated along the Newport-Inglewood, Palos Verdes, and San Clemente Faults and possibly additional faults [*Bennett et al.*, 1996]. The transfer of slip to the southern San Andreas Fault inland created a left step geometry at the latitude of the western Transverse Ranges, which because of the right-lateral relative plate motion, resulted in north-south shortening [*Bird and Rosenstock*, 1984]. The shortening has been accommodated at shallow levels by crustal convergence, which in the study area is manifested by active folding and thrust faulting along the northern edge of the Los Angeles Basin and the northern ICB [*Wright*, 1991; *Shaw and Suppe*, 1994]. A high P wave velocity anomaly in the upper mantle under the WTR and the San Gabriel and San Bernardino Mountains to the east has been interpreted to represent convective downwelling of subcrustal lithosphere which converged from north and south [e.g., *Humphreys and Hager*, 1990]. NE-SW compression due to a minor change in relative plate motion has been active in the ICB since the early Pliocene [*Ward and Valensise*, 1996], resulting in structural inversion [*Crouch and Suppe*, 1993; *Davis and Namson*, 1994; *Shaw and Suppe*, 1994] and the accentuated basin and ridge physiography of the ICB and Los Angeles Basin. Additionally, some of the offshore ridges (Palos Verdes, Catalina, and Lausen Knoll) could have been uplifted at gentle restraining bends along strike-slip faults, and others (San Clemente, elevated coastline between Los Angeles and San Diego) could have been uplifted by transpressional motion [*Mann and Gordon*, 1996].

3. Seismic and Gravity Data

Two offshore-onshore seismic lines, lines 1 and 2, oriented north-south and centered on the Los Angeles Basin at the epicenters of the 1933 Long Beach, the 1987 Whittier-Narrows, and the 1994 Northridge earthquakes, were recorded during the LARSE experiment [*Fuis et al.*, 1996, Figure 2]. Their offshore segments, 90 and 150 km long, respectively, were instrumented with ocean bottom seismometers (OBS) and PASSCAL Reftek stations on San Clemente and Catalina Islands [*Okaya et al.*, 1996; *ten Brink et al.*, 1996]. The R/V *Maurice Ewing*'s 20-element air gun array, totaling 137.7 L (8470 cubic inches), was used as a seismic source for the wide-angle seismic recordings [*Brocher et al.*, 1995]. These data were processed minimally, applying only band-pass filtering and predictive deconvolution. We also present here coincident multichannel seismic (MCS) reflection data, which were recorded along these lines by the *Ewing*'s 4.2-km-long, 160-channel digital streamer. Routine processing was applied to these data including Stoltz frequency-wavenumber (f-k) poststack migration. Coincident gravity data were recorded along lines 1 and 2 during the LARSE experiment by the *Ewing*'s KSS-1 marine gravimeter [*Brocher et al.*, 1995]. These and additional gravity data by the U.S. Geological Survey [*Snyder et al.*, 1982; *Langenheim and Jachens*, 1996] were used to check the seismic

results. In this paper we analyze the OBS data, a limited set of the wide-angle data recorded on the mainland and islands, and the MCS and gravity data.

4. Analysis of the Wide-Angle Seismic Data

The wide-angle seismic data throughout the study area show only two arrivals: *Pg*, upper crustal diving waves, and a strong arrival which we interpret as *PmP*, reflections from the Moho at critical and postcritical angles (Figure 4). Reflections and refractions from the sedimentary section are generally missing or appear as secondary arrivals, because sediments are localized in pockets (Figure 4). *Pg* arrivals are typically observed to maximum shot-receiver offsets of 50–60 km; however, *Pg* arrivals terminated at shorter offsets for shots fired to OBSs north of the Catalina Fault because energy traveling across the Catalina Fault was either dispersed or reflected back by the fault. *PmP* arrivals first appear at offsets of 40–50 km as delayed by ~1.5 s behind *Pg* arrivals. These offsets presumably represent the critical reflection point because reflection amplitude increases significantly as the critical point is approached. *PmP* arrivals can be followed to shot-receiver offsets of 160 km.

We believe that the arrival labeled *PmP* is indeed a postcritical reflection off the Moho and not an intracrustal reflection or a reflection from the top of a fossil oceanic crust, because of the following reasons: (1) The presence of a *Pn* arrival merging into this arrival on station L91 (Figure 4d) suggests that it is indeed a reflection off the Moho. Unfortunately, no other OBS or land record in the vicinity of the ICB shows *Pn* refractions, possibly because the rough bathymetry along both lines generates frequent shifts and delays in the arrivals, which tend to reduce their horizontal coherence. (2) The short critical offset of 40–50 km of the arrival requires a large velocity contrast. The smaller the velocity contrast across a reflecting boundary at a given depth, the larger the critical offset. Assuming a similar upper crustal model, a reflection off the top of a fossil oceanic crust with a velocity of 6.7 km/s would have a critical offset of ~65 km. (3) If this reflector is not *PmP*, we should observe a strong additional wide-angle reflection.

Bearing in mind that the lack of observation cannot constitute unequivocal evidence for the absence of a layer, we proceed with interpretation of these arrivals as representing a simple velocity structure which consists of a high gradient in the upper crust over a very low velocity gradient in the lower crust. The thickness of the low-gradient lower crust from the time delay between *Pg* and *PmP* is ~10 km. The location of the critical point for wide-angle Moho reflections at offsets of 40–50 km suggests a crustal thickness of the order of 15–25 km.

5. Tomography

Deriving a crustal velocity structure from the wide-angle reflection data involved several procedures. The main procedure was the application of a nonlinear travel time tomography which simultaneously inverts refraction and reflection travel times [*Zhang et al.*, 1998]. Here we give a brief overview of the tomographic method.

We used the shortest-path ray-tracing method [*Moser*, 1991]. This method expands a wave front in a velocity network from its source and calculates refraction and reflection travel times. The network consists of nodes arranged on the boundaries of grid cells, and each cell is assigned a constant velocity. The method involves three steps: timing nodes along an expanding wave front from a primary or a secondary source, finding a minimum travel time point along the wave front and taking this point as a new secondary source, and expanding a wave front from this minimum time point again. This method can correctly find diffractions, head waves, and paths to shadow zones. *Zhang and Toksoz* [1998] improved the numerical accuracy and efficiency of the method by optimizing the node distribution on the cell boundaries to yield uniform angle intervals. For LARSE line 1 we discretized a two-dimensional (2-D) profile, 90.2 km long and 24.6 km deep into 1100 × 300 grid cells with a spacing of 82 m resulting in 330,000 cells. For LARSE line 2 we discretized a 2-D profile, 160.5 km long and 25.0 km deep, into grid spacing of 100 m, resulting in 401,250 cells. The initial model consisted of fixed seafloor topography and water velocity and a constant half-space subseafloor velocity of 2 km/s.

No matter how sophisticated the optimization approach is, there can be no definitive "solution" based solely on fitting the travel time data. Two constraints are added to improve the reliability of the solution [*Zhang et al.*, 1998]: (1) Travel time is inverted in the forms of both average slowness (travel times divided by ray lengths) and apparent slowness (travel time derivatives with respect to distance). By using apparent slowness data in the tomography problem we treat the travel times as curves rather than uncorrelated points, thus fitting data in a more physically meaningful way. (2) A smoothness constraint on the slowness model is explicitly incorporated as part of the global inversion to find the simplest structure solution (the smoothest solution) that fits the data to within a given tolerance. The objective function, minimized using the conjugate gradient method, thus consists of an average slowness term, an apparent slowness term, and a smoothness term.

To calculate reflection travel times, we expand a wave front from the source and time the nodes in the slowness network which are at or above a given reflector [*Zhang et al.*, 1998]. The first-arrival refraction travel times and the minimum travel times from the source to a given reflector are determined simultaneously. Then we continue to expand a wave front only from the reflector (which acts as a line source) back to the receivers by assigning infinite travel times to the rest of the network nodes.

6. Results

6.1. Shallow Structure, Faulting, and Deformation

Near-surface velocity highs are correlated with the location of known basement ridges and knolls such as the San Clemente and Catalina Ridges and the Emery and Avalon Knolls, which are devoid of well-stratified sediments on coincident MCS data (Plates 1a and 1b). A basement high (Figure 5a) under the shelf edge on line 1 is probably made of Catalina Schist [*Wright*, 1991]. If the northern limb of the basement high on line 1 is a detachment fault, then the Palos Verdes Fault merges down into a possible detachment of the kind cited farther south along the coast as an indication for a metamorphic core complex [*Crouch and Suppe*, 1993]. On line 2 the Palos Verdes Fault merges downward into a concave reflection (Figure 5b) and a contrast in the velocity field along the northern limb of a "basement" high at the shelf edge on line 2 (Plate 1b). However, this surface might not represent a low-angle detachment fault, because the basement high (which should represent the lower plate) is made of tightly folded Monterey

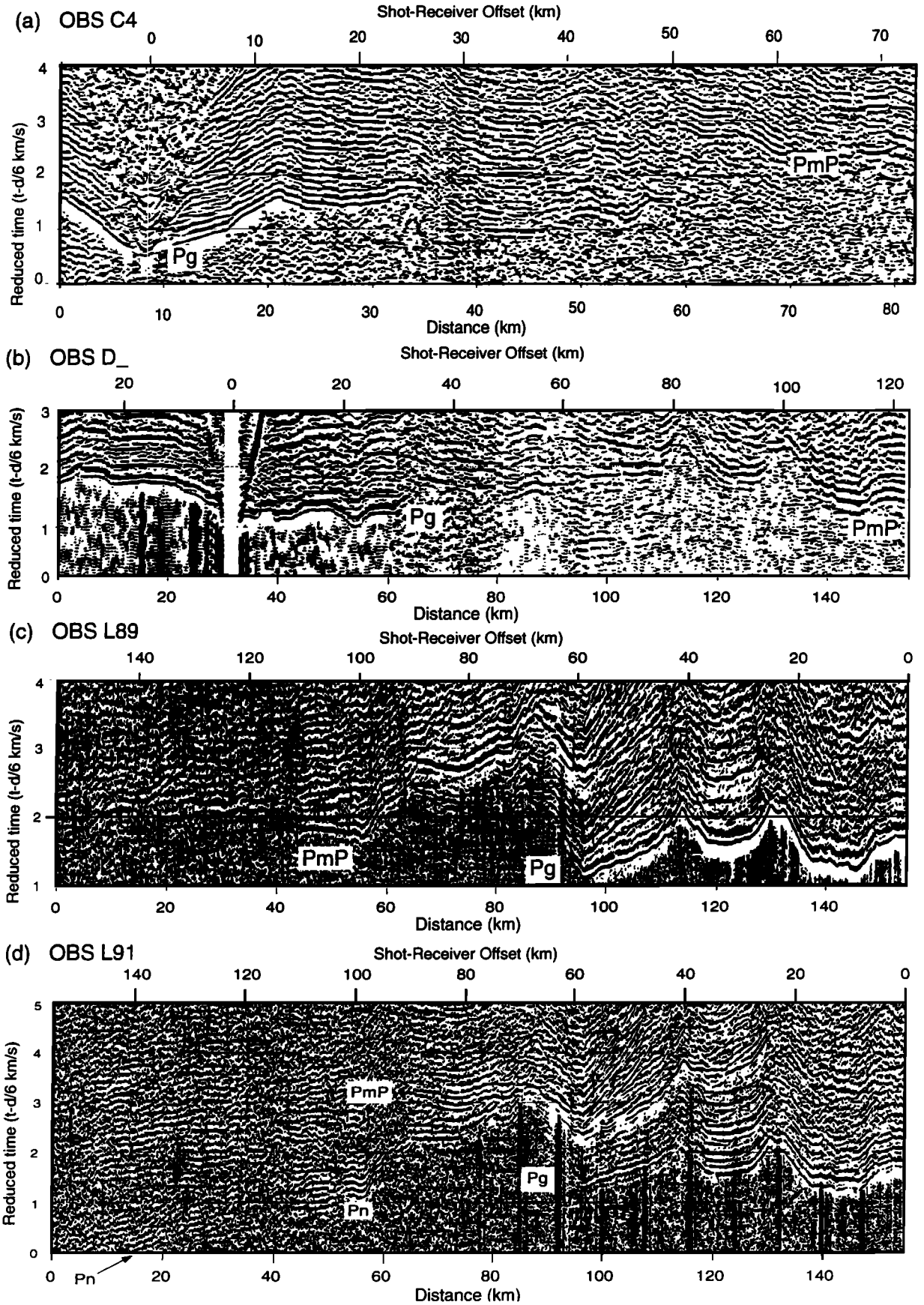

Figure 4. Examples of wide-angle seismic data: (a) line 1, OBS C4; (b–d) line 2, OBS D_, L89, and L91. Linear move-out of 6 km/s, spiking deconvolution, band-pass filter between 4 and 20 Hz, and automatic gain control were applied to the data.

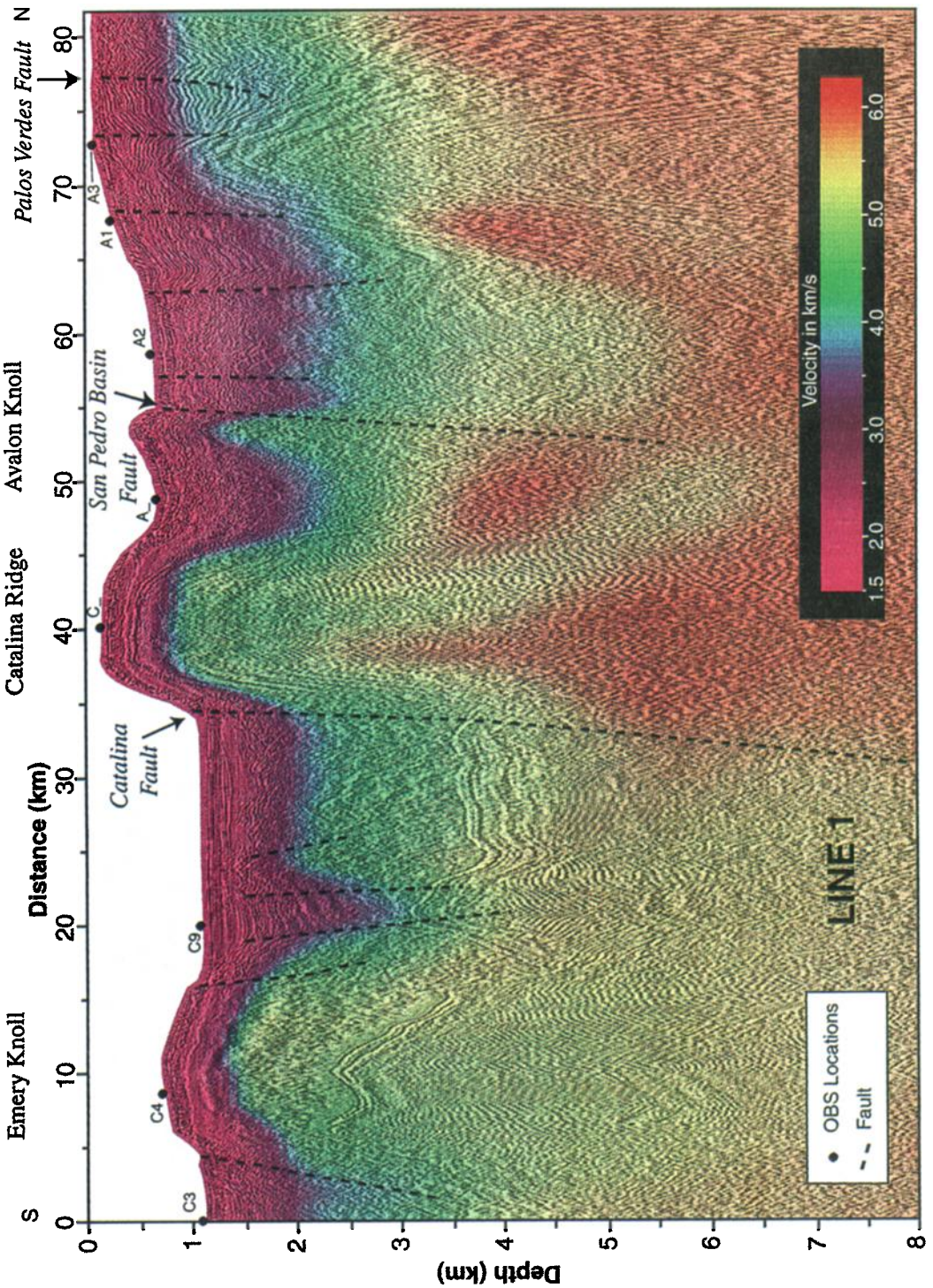

Plate 1a. Depth-converted MCS profile along line 1 with color overlays of the velocity model from tomographic solution of the wide-angle seismic data (Plates 2a and 2b). Velocity model was also used to convert the MCS profile from time to depth. Vertical exaggeration is ~7:1. Dashed lines show possible fault traces interpreted from combined reflection geometry, velocity model, and known surface fault location. Black circles show location of OBS. A misfit between velocity and reflections showing a sedimentary sequence at the north end of line 1 (75–82 km) is due to lack of ray coverage in the refraction data.

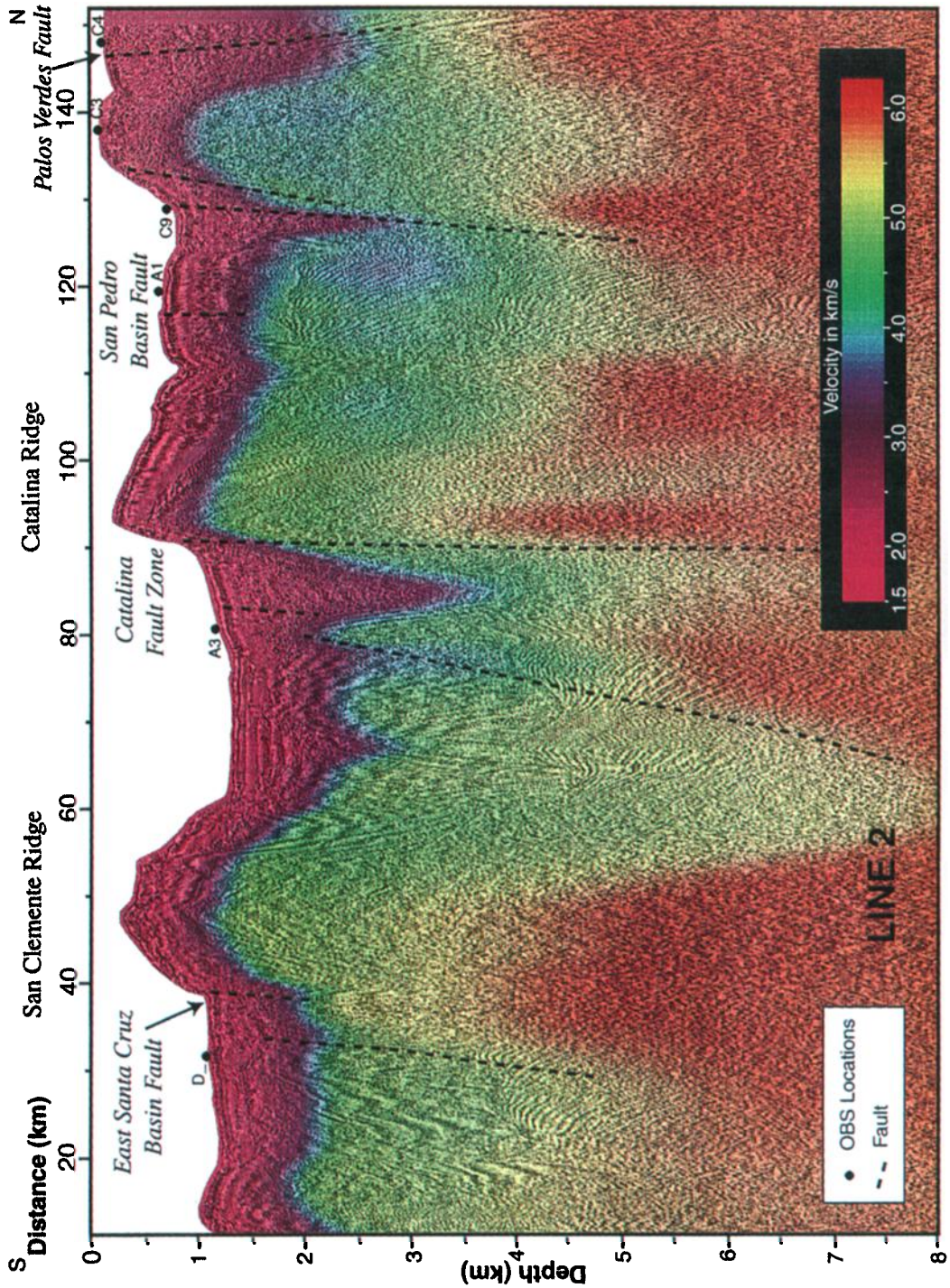

Plate 1b. Same as Plate 1a, except for line 2. Vertical exaggeration is 12.5:1.

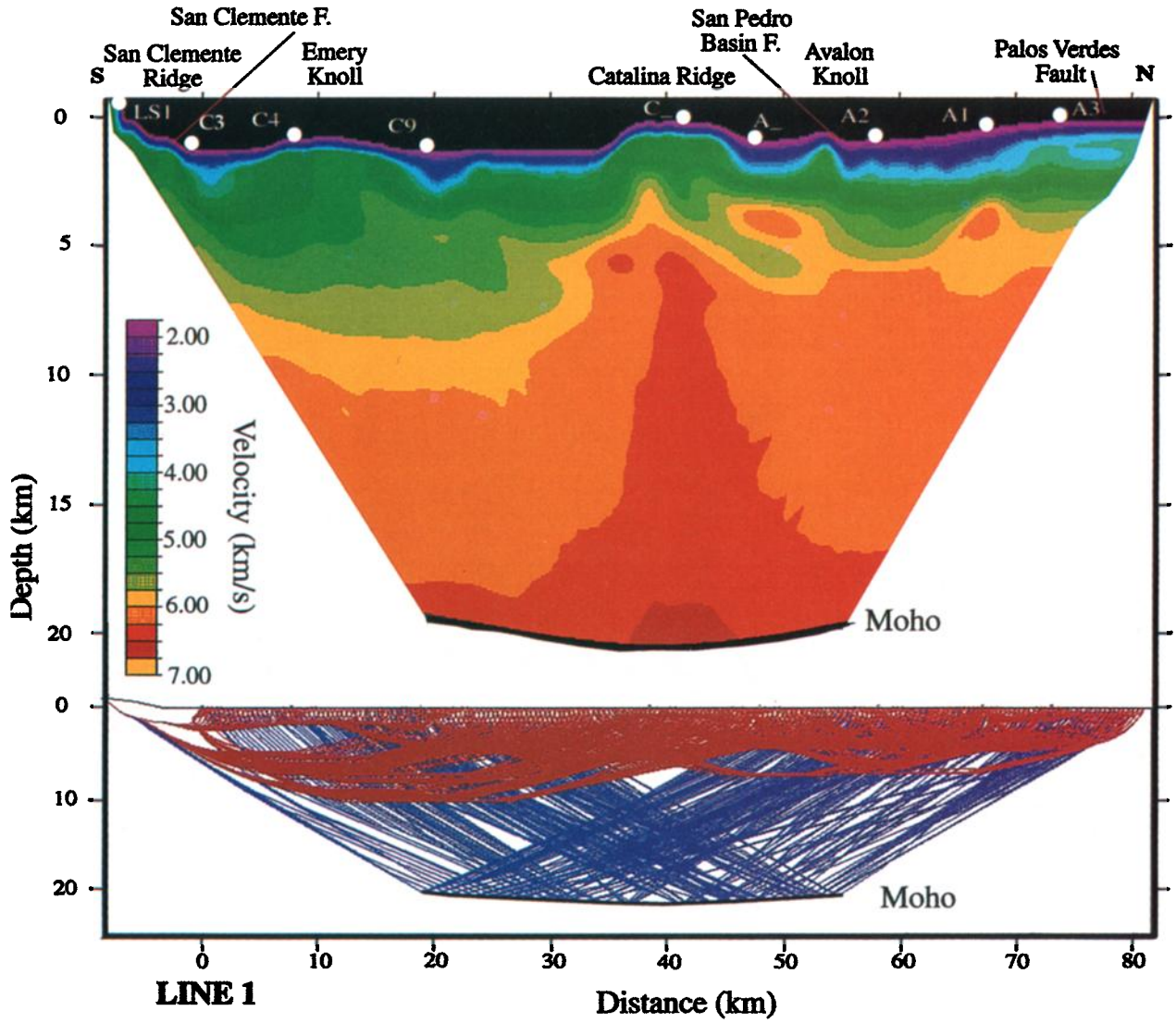

Plate 2a. (top) Tomographic solution for line 1. (bottom) Ray coverage: red, upper crustal refractions (Pg); blue, Moho reflections (PmP). White circles, locations of seismic stations. Vertical exaggeration is 3.5:1 for the velocity model.

shales whose age overlaps ICB extension [*Junger and Wagner*, 1977; W. Normark, personal communication, 1998]. On both lines the Palos Verdes Fault has a thrust component; on line 1 (Figure 5a) the fault surface dips southward, similar to previous interpretation [*Wright*, 1991; *Shaw and Suppe*, 1996], but on line 2 it dips in the opposite direction (Figure 5b), contrary to *Wright*'s [1991] interpretation.

Farther seaward along line 1, inferred Cenozoic sedimentary rocks are tightly folded and faulted under the San Pedro Basin (Plate 1a and Figure 5a). Deformation in some areas extends up to the seafloor. A major example is the San Pedro Basin Fault [*Junger and Wagner*, 1977]. Apparent thrust dip of these faults is NE on the shelf's slope and SW farther westward. This change may indicate reactivated normal faults (Figures 5a and 5b). Thrust faults and overlying folds in deep water farther south were interpreted to merge into a low-angle detachment fault [*Bohannon and Geist*, 1998]; however, our refraction and reflection data in deep water (Plate 1a and Figure 5a) do not support a similar interpretation here.

The Catalina Fault is associated with a large seafloor escarpment on the MCS data (Figures 5a and 5b) and a horizontal velocity discontinuity to a depth of ~10 km in the velocity model (Plates 2a and 2b). On line 1 the fault consists of a single trace, whereas in line 2 there appears to be also deformation zone west of the escarpment, which may be the continuation of the fault on line 1. This geometry may be due to en echelon configuration of the Catalina Fault between lines 1 and 2 (Figure 2). The basin between the two fault strands may have been originally a pull-apart basin, which under a later compressional regime is being internally folded and is tilted away from the main escarpment.

Upper crustal velocities under both lines 1 and 2 are characterized by a high velocity gradient extending from the seafloor to depths of 4–10 km (Plates 2a and 2b). Velocity gradient is lowest under the Catalina Basin where velocities <6 km/s extend to 10 km depth. The gradient is intermediate west of San Clemente Ridge (line 2) and highest under San Pedro Basin and the continental shelf, where gradients reach 0.75

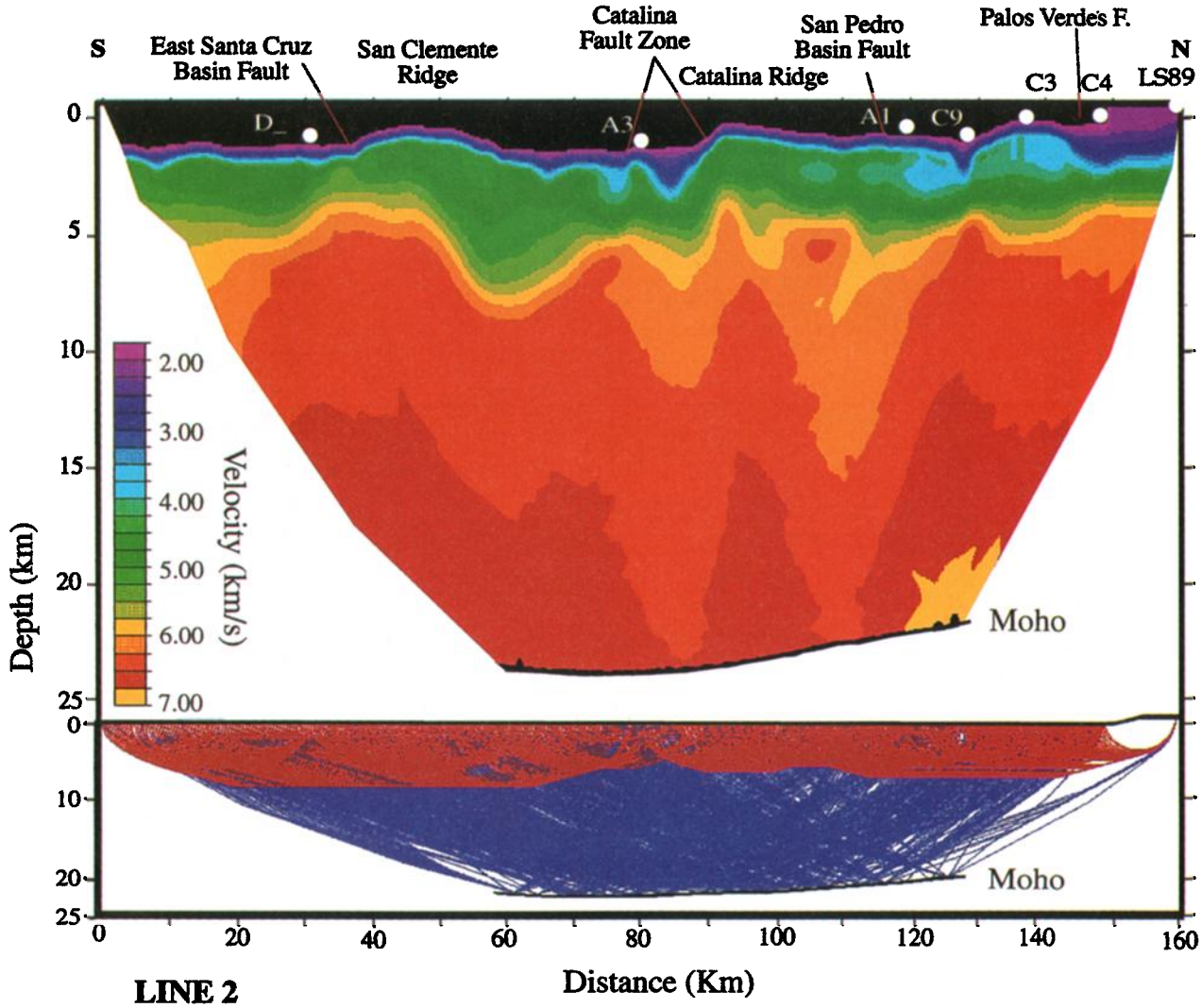

Plate 2b. Same as Plate 2a, except for line 2. Vertical exaggeration is 4.5:1 for the velocity model.

km/s/km at depths of 2–4 km. Disruption of the seafloor and shallow subsurface on MCS lines 1 and 2, indicating recent deformation, extends as far westward as the Catalina Fault zone. It is coincident with the region of high upper crustal velocity gradient, although most small to moderate earthquakes ($3 \leq M_w \leq 5$) lie west of the San Pedro Basin Fault.

Superposition of the velocity field on the depth-converted seismic reflection profiles (Plates 1a and 1b) suggests that the stratified reflections in San Pedro Basin, north of San Clemente Fault, north of Emery Knoll (line 1), and in the San Pedro and Catalina Basins (line 2) are low-velocity (<3.5 km/s) sedimentary rocks. The velocity is similar to the range of *P* wave velocity of Pliocene and Miocene formations from the Los Angeles Basin and San Gabriel Valley, derived from sonic logs [*Brocher et al.*, 1998]. These sediments also have low densities: A negative gravity anomaly (−30 to −50 mGal) is observed over the Santa Monica Basin (Figure 6), where the thickest post-Miocene strata in the ICB are located [*Vedder*, 1987]. Large amplitude variations in the observed gravity between 100 and 140 km on line 2 can only be fit if sediment density is 1200–1600 kg/m^3 (Figure 7) or if out-of-plane effects are considered.

6.2. Deep Structure

The crustal velocity structure below a depth of 8–10 km is determined solely from matching the range of move-out of *PmP* arrivals. Within the limited resolution of such data the middle and lower crust is relatively homogenous within each line, with the exception of the crust under Catalina Ridge, which is ~5% faster than adjacent crust (Plates 2a and 2b). The average crustal velocity below 8 km is 6.3 km/s for line 1 and 6.5 km/s for line 2. The offshore ray coverage allows us to locate the Moho only under the center of the profiles. The Moho is at 19–20 km depth under line 1 and 22–24 km depth under line 2 (Plates 2a and 2b). Data from four land stations at the northern end of line 2 were modeled using a two-point forward ray-tracing scheme [*Zelt and Smith*, 1992] to extend the determination of Moho depth northward. This model shows the crust thinning northward slightly until it reaches the base of the continental shelf at model kilometer 135, where it thickens again (Figure 8). The thin crust under the ICB contrasts with a crustal thickness of 30–35 km in mainland southern California [*Hearn and Clayton*, 1986; *Sung and Jackson*, 1992; *Ryberg and Fuis*, 1998]. It appears to maintain a fairly

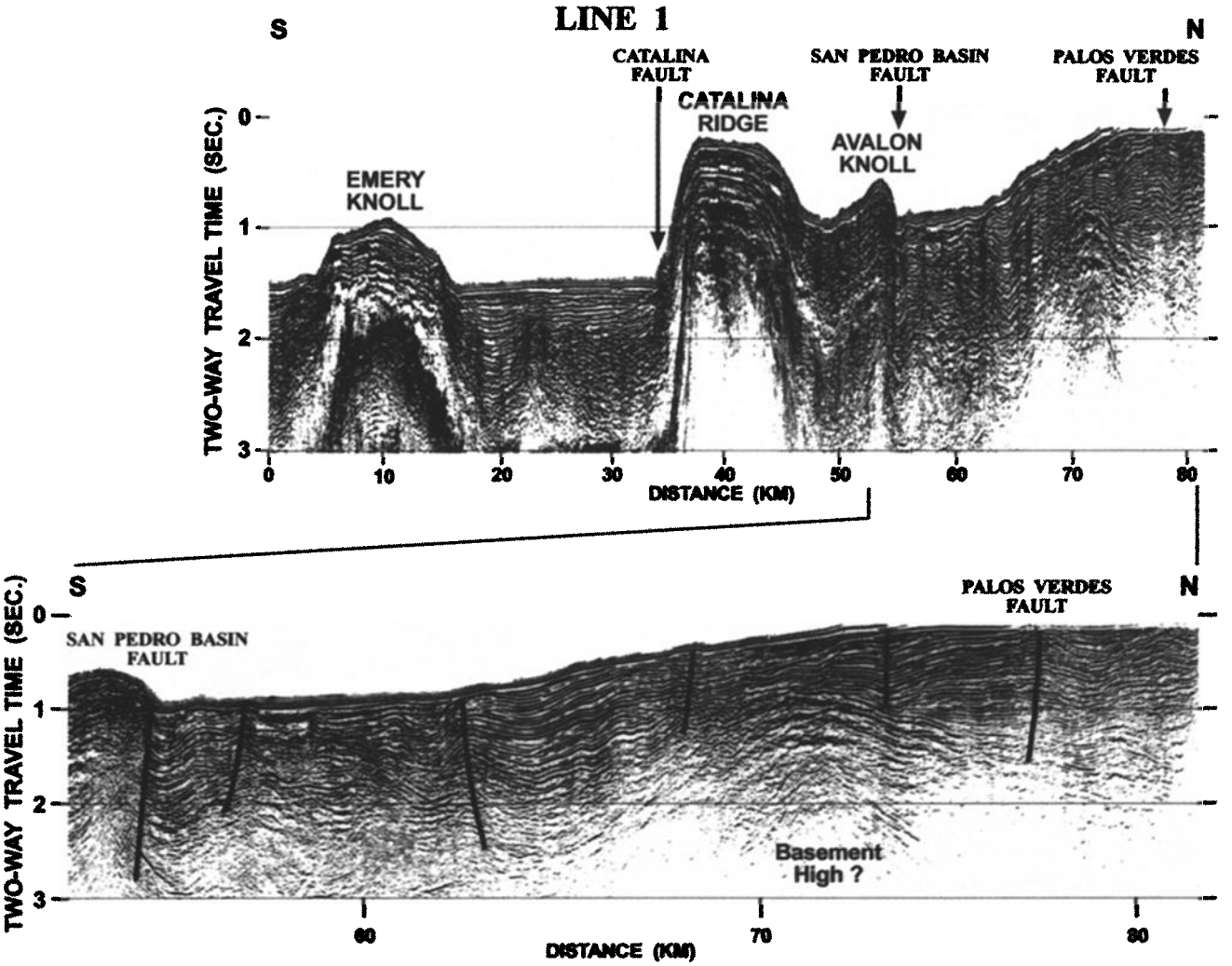

Figure 5a. Coincident MCS profile for line 1 with enlargement showing the northernmost nearshore parts of the lines. Stoltz f-k poststack migration was applied.

uniform thickness to the shelf slope. Independent geological and shallow seismic reflection data also place the ICB–western Transverse Ranges boundary under the shelf [*Crouch and Suppe*, 1993]. Gravity data, discussed in section 6.3, indicate that the transition is abrupt.

Ray tracing of the only observed *Pn* arrival in the data from line 2, a single unreversed station (L91), gives an upper mantle velocity of 7.7–7.9 km/s (Figures 4a and 8), similar to upper mantle velocity under the western Transverse Ranges [*Hearn and Clayton*, 1986]. Note that in order to fit the *Pn* arrival at far shot-receiver offsets we needed to create a step in crustal thickness under San Clemente Ridge (Figure 8). Although this step coincides with the boundary between the ICB and the OCB, it is based on a single unreversed record and therefore should not be interpreted geologically.

The differences in crustal velocity between the two lines could be attributed to an ambiguity between the average crustal velocity and depth to the Moho (i.e., if we place the Moho deeper, we have to increase the average crustal velocity to fit the observed travel time) and therefore could be interpreted to represent the resolution of the model. We believe that the large move-out range for *PmP* (45–80 km on line 1 and 45–160 km on line 2) sufficiently constrains the average crustal velocity. In addition, the vertical incidence two-way travel time to the Moho under Catalina Ridge was calculated from the tomographic model of line 1 and compared to the travel time of the most prominent deep reflection in the MCS data. The calculated travel time from the tomography model matches this prominent reflector to within 0.1 s (Plate 3). The MCS data were processed completely independently from the wide-angle data, including the derivation of stacking and migration velocities, yet yield the same depth to Moho.

The Bouguer gravity anomaly over Catalina Ridge (Figure 6) is in agreement with observed variations in crustal velocity between the two lines. The anomaly is 6 mGal lower on line 2 than on line 1. A 3-km-thicker crust under line 2 than under line 1 with a 350 kg/m^3 density contrast across the Moho yields a 44 mGal difference. However, if the lower crust is also slightly denser under line 2, for example, by 92 kg/m^3 in the lowest 10 km of the crust, then the calculated anomaly is only 6 mGal lower, as observed. The higher density corresponds to a 0.21-km/s-higher average velocity [*Christensen and Mooney*, 1995], as observed.

Crustal imaging by the seismic reflection method during LARSE was largely unsuccessful, similar to previous attempts [e.g., *Bohannon and Geist*, 1998; *Crouch and Suppe*, 1993],

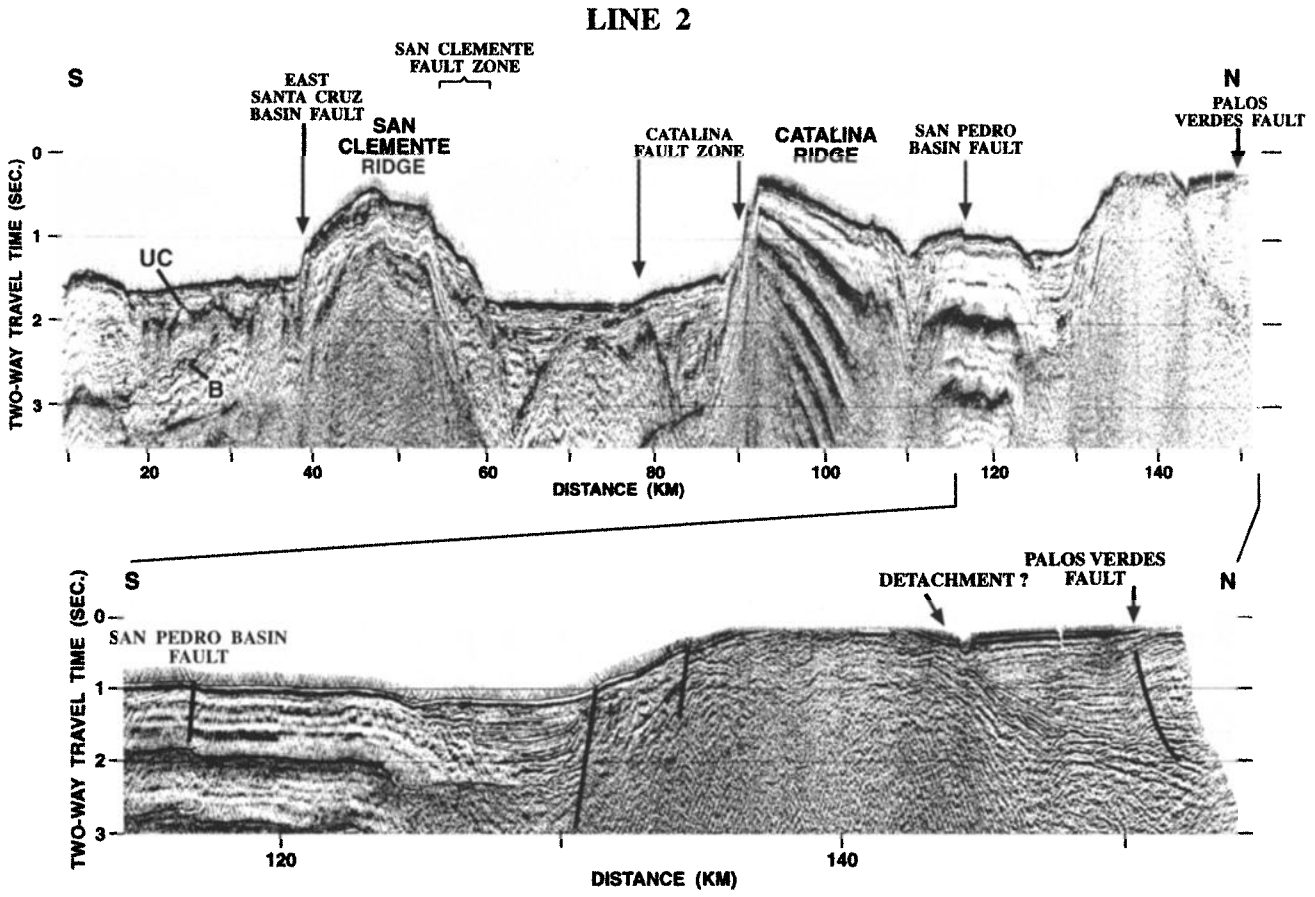

Figure 5b. Same as Figure 5a, except for line 2. UC, unconformity; B, basement reflector.

probably because of diffraction of the seismic energy by the Catalina Schist and large-amplitude seafloor multiple reflections. An exception was the Catalina Ridge under line 1, where the amplitudes of these multiples decayed after a few seconds and lower crust (>10 km depth) and Moho reflections can be observed (Plate 3).

6.3. Boundaries of the ICB

We use the gravity field to help constrain the shape of the lateral crustal thickness change from the ICB to the western Transverse Ranges. The seismic model derived from land seismic stations L94 and L99 suggests that crustal thickening starts at the base of the continental shelf (135 km in Figure 8). Crustal thickness under the western Transverse Ranges may reach 30 to 35 km but is not well constrained [*Hearn and Clayton*, 1986; *Sung and Jackson*, 1992]. The gravity model best fits the data with a thickness change occurring within a ≤25-km-wide zone (Figure 7). If the change occurs more gradually, over 50 km, the calculated gravity anomaly overestimates the observed anomaly at the shelf and coast. If the change is abrupt, over 5 km, the calculated gravity anomaly underestimates the observed anomaly at the shelf and coast, but it improves the fit over the Santa Monica Basin (103–143 km on line 2). In map view the boundary of the western Transverse Ranges with the ICB and the Los Angeles Basin is characterized by a pair of E-W trending low and high Bouguer gravity anomalies (Figure 6). This paired anomaly is due to upper crustal density anomalies associated with the Ventura Basin and with the Santa Monica Mountains and Santa Cruz Island south verging thrusts, respectively.

The location and the geometry of the boundary between the ICB and the Los Angeles Basin are less clear. Unpublished onshore-offshore refraction results of Y. G. Li and D. Okaya [*Bohannon and Geist*, 1998] and preliminary forward modeling of *Pg* and *Pn* arrivals along land stations of line 1 (G. S. Fuis et al., manuscript in preparation, 1999) suggest that the Moho deepens abruptly near model kilometer 70, beneath the continental slope (Figure 7a). From this location the Moho dips landward at ~9°, assuming an upper mantle velocity of 8 km/s [*Kohler and Davis*, 1997]. Catalina Schist rocks in drill holes are encountered only west of the Newport-Inglewood Fault [*Wright*, 1991]. The maximum depth of earthquakes is usually shallower west of the fault, suggesting a change in crustal rheology across that fault from felsic (Catalina Schist) to more mafic crustal composition [*Magistrale and Zhou*, 1996].

The boundary between the ICB and OCB is manifested on the Bouguer gravity map (Figure 6) as higher gravity anomaly over the OCB with respect to the ICB. The difference may be due either to a thinner low-density sediment cover, to a thinner crust, or to an increased crustal density of the OCB. Variations in the thickness of the low-density sediment cover are an unlikely explanation, because the differences in gravity between the two provinces are found even in areas which are devoid of post-Miocene sediments. A thinner crust under the OCB cannot be ruled out as an explanation because crustal thickness there is unknown except for the Patton Ridge at the outermost

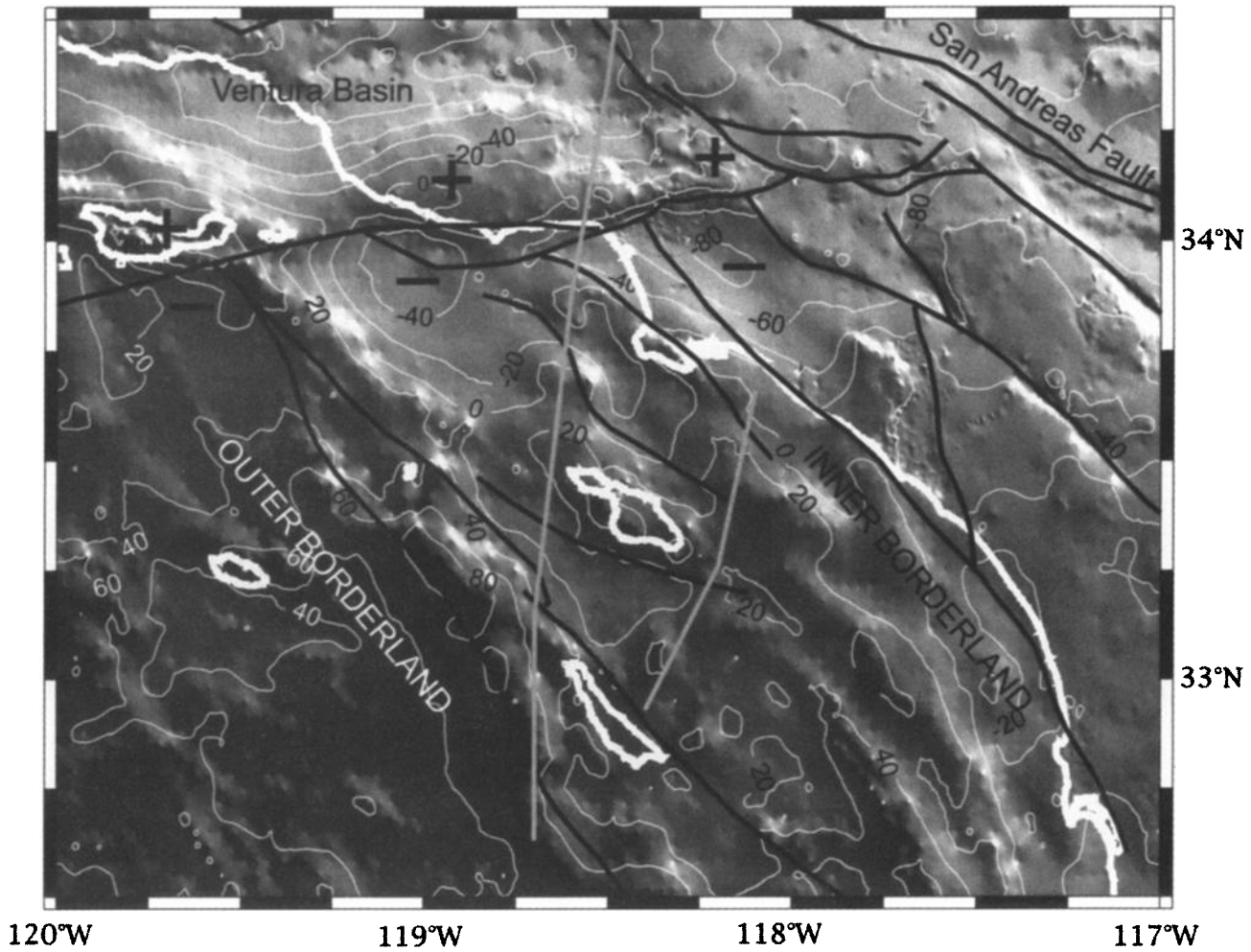

Figure 6. Grey-shaded and contoured Bouguer gravity map of southern California with illumination from the NE. Heavy white lines, coast. Grey lines, locations of gravity profiles in Figure 7. Heavy solid lines, major faults. Plus and minus signs, gravity maxima and minima along the southern boundary of the WTR.

edge of the OCB [*Shor and Raitt*, 1958]. A higher average crustal density in the Outer Borderland is also a plausible explanation for the higher gravity values there. Geological evidence suggests that the OCB is in part underlain by higher-density Great Valley forearc crust [*Vedder*, 1987]. In the Great Valley this forearc crust has an average crustal velocity of 6.5–7.0 km/s and an average density of >2950 kg/m^3 [*Godfrey and Klemperer*, 1998].

A shallow high-velocity (5.1–6.0 km/s) region under San Clemente Ridge on line 2 is offset southward from the surface expression of the San Clemente and the Eastern Santa Cruz Basin Faults (Plates 1b and 2b). This high-velocity anomaly coincides with a positive magnetic anomaly that was interpreted to arise from a shallow magmatic intrusion [*Harrison et al.*, 1966]. A 75-km-long NW-SE trending positive Bouguer gravity anomaly which does not correlate with the bathymetry can also be observed in this area between San Clemente and Santa Barbara Islands (Figure 6). The source of the high-velocity, high-density, and high-susceptibility anomalies may be a mid-Miocene magmatic complex because volcanic flows of similar age are exposed on San Clemente Island. Alternatively, the source of the velocity and density anomalies at shallow crustal levels may be ophiolites, because dredges from the center of the gravity high exposed Jurassic ophiolitic rocks [*Vedder*, 1987].

The area SW of San Clemente Ridge on MCS line 2 (Figure 5b) is characterized by a different sedimentary sequence than north and east of the ridge, supporting the interpretation that this area is part of the OCB [*Crouch and Suppe*, 1993]. A smooth, high-amplitude reflector, probably basement, dips southward. Weak layered reflections representing sediments appear to pinch out northward and are truncated by an erosional unconformity. The overlying sediments are generally flat lying but are locally disturbed, probably because of slumping or mass wasting. Using correlations with nearby wells, *Bohannon and Geist* [1998] interpret the sediments below the erosional surface as forearc strata which are the equivalent to the Great Valley sequence in central California and the overlying sediments as lower to middle Miocene strata. If these ages are correct, there appears to be little post-Miocene tectonic activity west of San Clemente Ridge.

7. Discussion

7.1. Crustal Structure and Extension Modes in the ICB

The seismic structure of the ICB crust is characterized by the following observations: (1) Localized pockets, <2 km thick, of low-velocity sediments, (2) relatively high upper crustal velocity averaging 5.7 and 5.6 km/s for lines 1 and 2, respectively, (3)

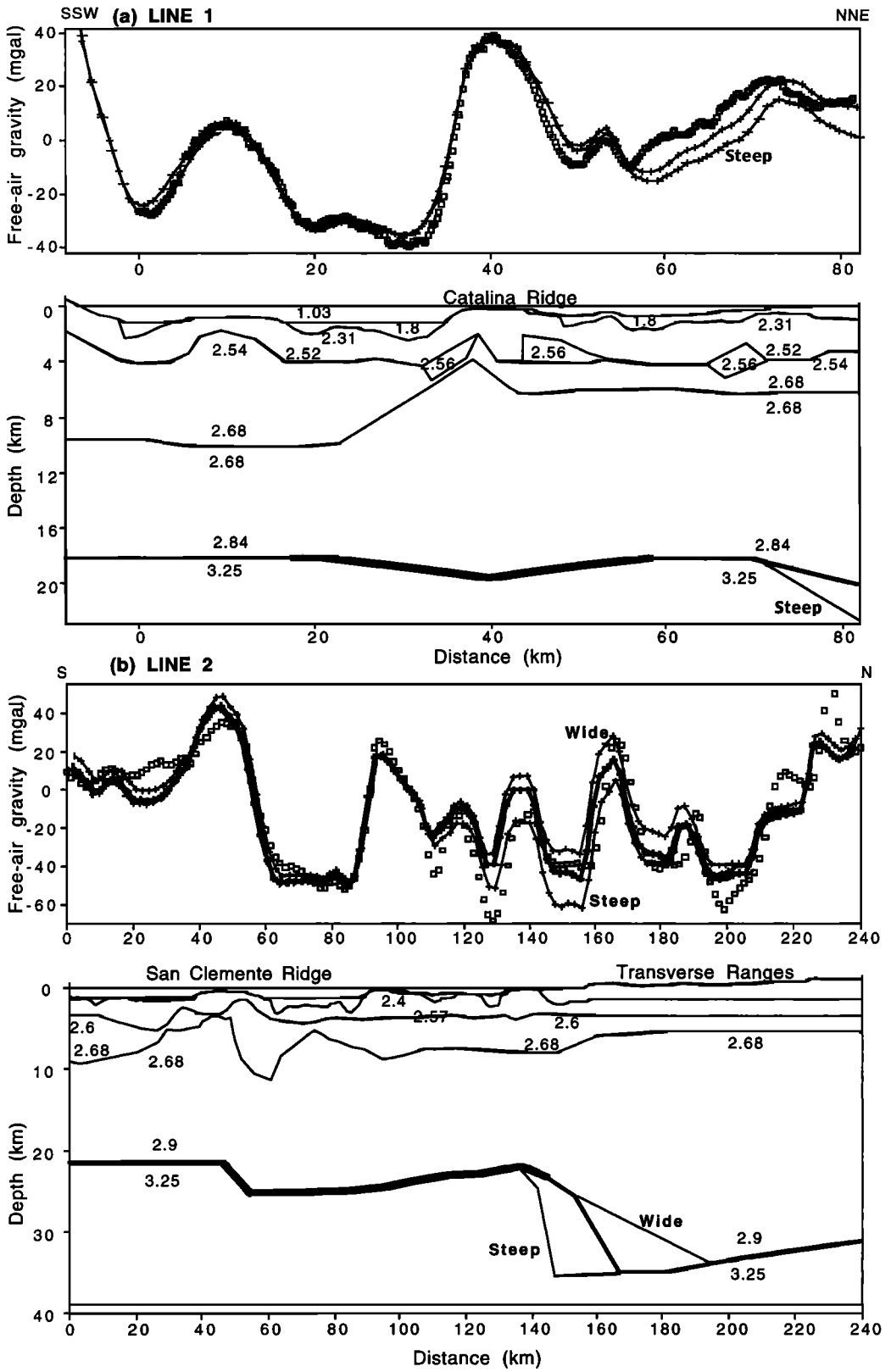

Figure 7. Gravity profiles along (a) line 1 and (b) line 2. Observed gravity values are plotted as squares; calculated profiles are in various patterned lines. The profile of line 2 was extended 80 km northward (see Figure 6 for location) to model the transition between the California Inner Continental Borderland and the western Transverse Ranges. Heavy line, Moho geometry inferred from seismic data. Perturbations to the geometry of the transition from ICB to WTR ("Wide" and "Steep") and the corresponding predicted gravity anomaly are shown on line 2. Velocity-density ratios are after *Hamilton* [1978] for $V_p \leq 5.5$ km/s and *Christensen and Mooney* [1995] for $V_p > 5.5$ km/s. Lower crust and upper mantle densities are laterally uniform in these models, although velocities may vary laterally by 5%.

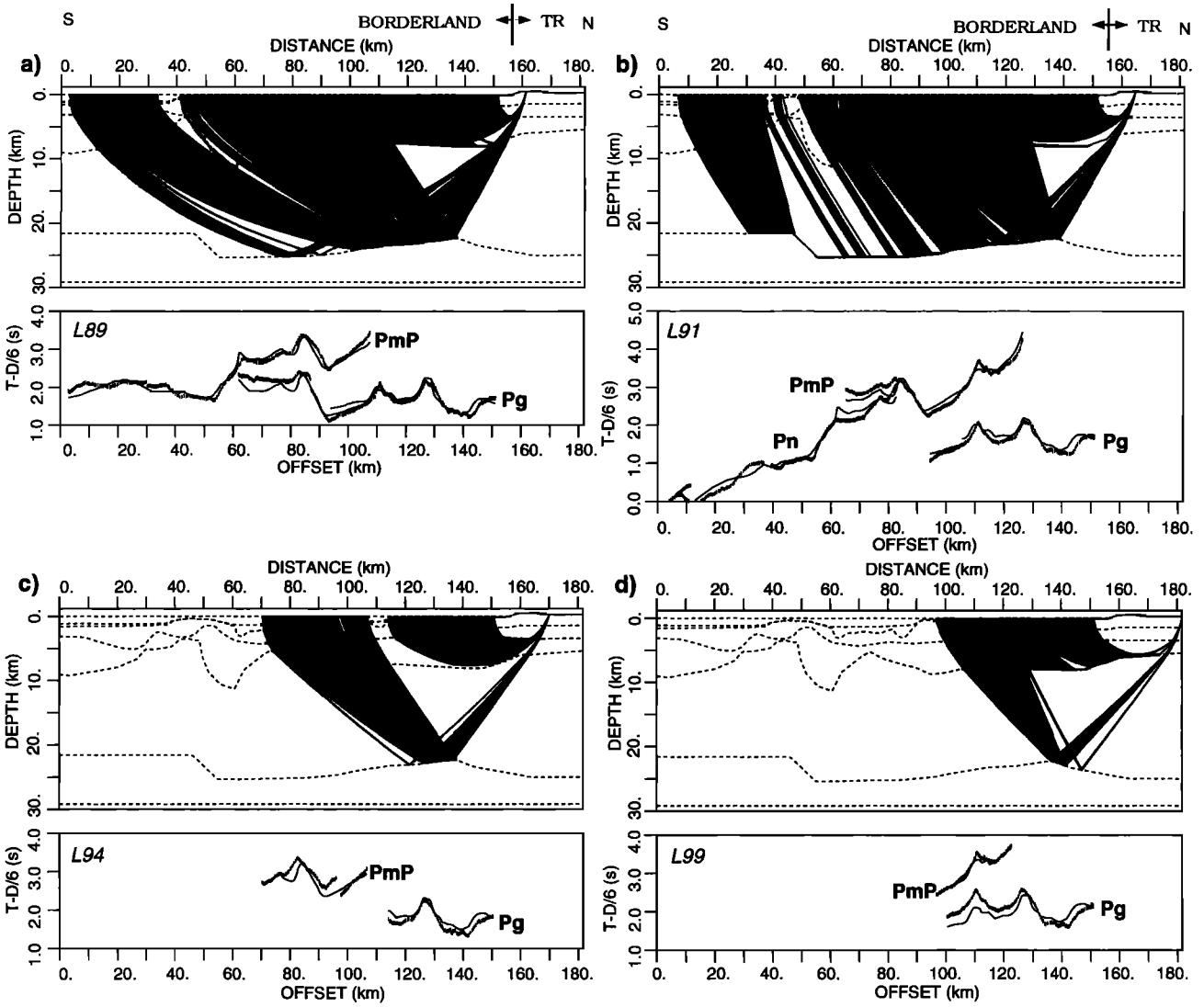

Figure 8. Forward two-point ray-tracing model and ray coverage [*Zelt and Smith*, 1992] for land stations at distances <30 km north of the northern end of line 2. Bottom of each model shows comparison between observed and calculated travel times. TR, Transverse Ranges. $T - D$, time minus distance.

homogenous P wave velocity averaging 6.3 and 6.5 km/s for lines 1 and 2, respectively, for the crust below 8 km depth, (4) relatively flat Moho at 19–20 and 22–23 km depth for these lines, respectively, (5) weak fine-scale reflectivity between 4 and 7 s two-way travel time under Catalina Ridge, and (6) no indication in either the wide-angle data or the MCS data for a high-velocity layer at the base of the crust.

The average velocity for line 1 in the depth range of 4–15 km is within 0.1 km/s of laboratory-measured P wave velocity of metamorphic rocks of Franciscan origin, the Pelona Schist; and that of line 2 is 0.25 km/s higher [*McCaffree-Pellerin and Christensen*, 1998; N. Christensen, personal communication, 1999]. Catalina schist is inferred from dredges and wells to underlie most of the ICB [e.g., *Vedder*, 1987]. Outcrops of the Catalina Schist consist entirely of medium to high–pressure and –temperature metagreywacke and metavolcanic rocks which originated at an accretionary prism (summaries by *Vedder* [1987] and *Crouch and Suppe* [1993]). Hence we interpret the crustal velocity structure to indicate a crust made almost uniformly of Catalina Schist. Average crustal velocities for lines 1 and 2 increase faster than laboratory-measured Pelona Schist at depth >15 km, suggesting the presence of a larger percentage of intrusive or preexisting crust in the lower crust.

Compared with other locations along the west margin of North America, our preferred crustal velocity model of the ICB is unusual because it has a thin low-velocity cover and no basal high-velocity layer. Seismic sections along the California margin from the Santa Barbara Channel immediately north of the ICB to San Francisco are characterized by a high-velocity basal layer (>6.5 km/s) which is separated by a velocity discontinuity from the overlying crust [*Crandall et al.*, 1983; *Brocher et al.*, 1999]. Two to three kilometers of low-velocity sediments usually top these crustal sections. The seismic structure of the Great Valley forearc sequence comprises several kilometers of low-velocity sediments overlying high-velocity (6.5–7.5 km/s) crust [*Godfrey and Klemperer*, 1998]. If these sections typify the fossil accretionary prism and forearc regions of the California subduction system, then the crustal section in the ICB has lost its overlying lower velocity sediment and crustal layers and its basal high-velocity part. The total crustal thick-

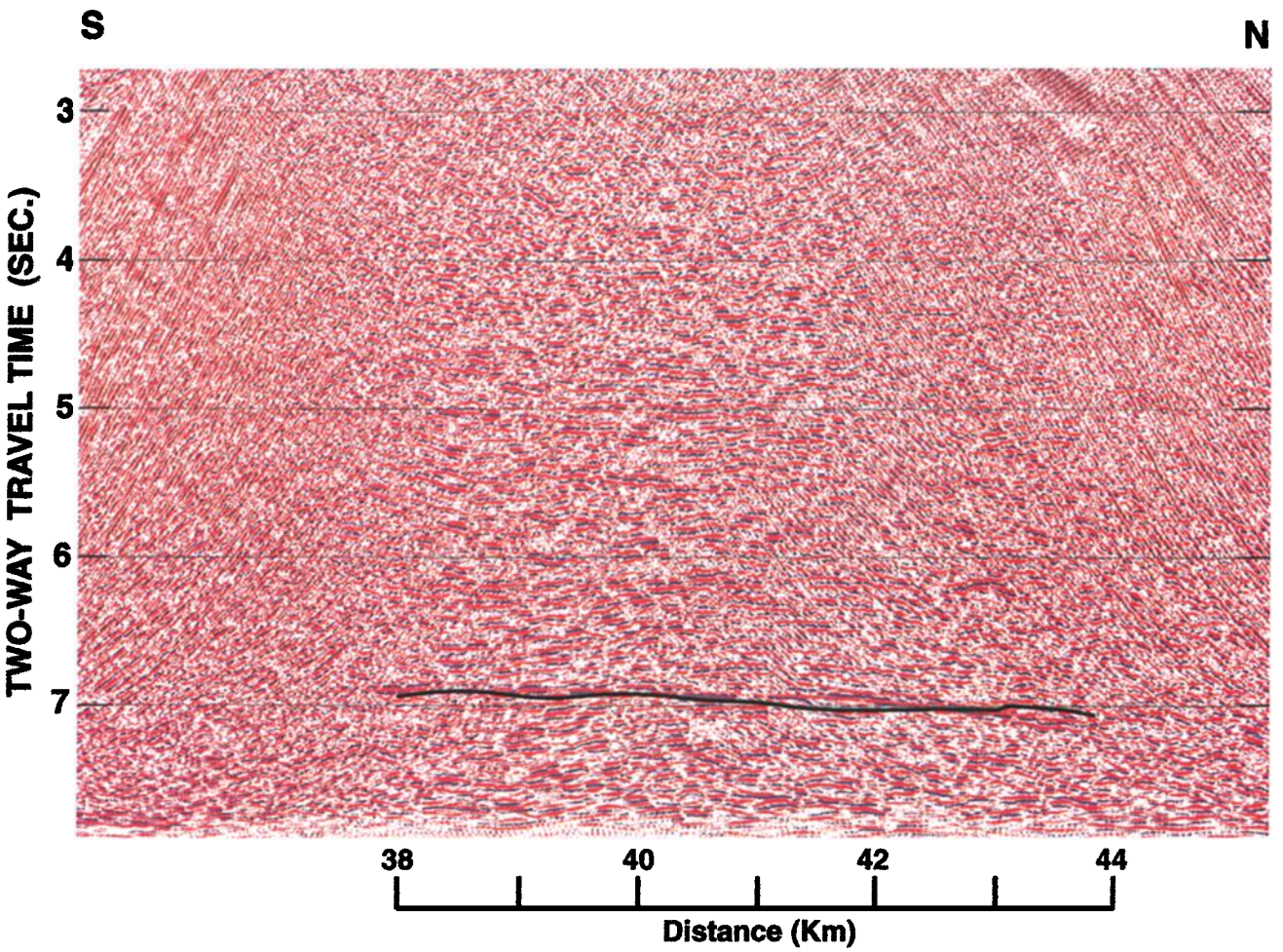

Plate 3. Enlargement of the lower part of MCS line 1 under Catalina Ridge. Heavy line indicates the calculated two-way travel to the Moho from the tomographic model.

ness of the ICB is also unusually thin and does not include higher velocities compared to global compilations of crustal velocity structure [*Christensen and Mooney*, 1995].

The near absence of sediments despite the location of the ICB in the former forearc probably indicates removal of the upper crustal section, which is in agreement with the suggestion that Catalina Schist was exhumed from depths of 10–15 km during the Miocene [*Crouch and Suppe*, 1993]. Other evidence for subaerial exposure of the ICB includes the following: (1) The widespread San Onofre Breccia is derived from Catalina Schist along its eastward boundary with the Peninsular Ranges and its northward boundary with the western Transverse Ranges [*Stuart*, 1979]. (2) The later part of the Conejo volcanics appears to have been erupted subaerially [*Hurst*, 1982]. Faunal evidence within the tuff suggests that some of these have erupted at elevations >1300 m above sea level [*Stadum*, 1998]. (3) The earliest sediments within the ICB only date back to the later part of the Miocene. Their fossil assemblage indicates initial deposition in shallow water and deposition in bathyal depths occurring only toward the end of the Miocene and in the Pliocene [*Vedder*, 1987]. Seismic and well data in the physiographically similar OCB, on the other hand, show 1000–3000 m of pre–Middle Miocene sediments (*Bohannon and Geist* [1998]; southernmost end of line 2, Figure 5b).

Isostatic considerations require that lithospheric extension be accompanied by surface subsidence, not uplift and exhumation, unless material is added to the crust during extension, the density of the crust is significantly modified, or mantle buoyancy is provided. Crustal thickening during the formation of core complexes was suggested to be partially achieved by the addition of mantle-derived material to the base of the crust [*Gans*, 1989; *Hill et al.*, 1995]. However, despite abundant volcanism at the ICB and its margins, there does not seem to be a high-velocity basal layer or strong crustal reflections corresponding to mafic magmatic bodies within the crust. *McCarthy et al.* [1991] also noted that despite abundant syntectonic magmatism during extension of Basin and Range metamorphic core complexes, low seismic velocities are recorded throughout the crust. Our seismic results are more compatible with the suggestion of a regional-scale flow in the lower crust into the region [*Block and Royden*, 1990]. The material which flowed into the ICB was probably metamorphosed Mesozoic Franciscan subduction complex rocks which underlay parts of southern California [*Crouch and Suppe*, 1993].

Uplift of the surface of the ICB could also be partially achieved by changing the average crustal density during crustal replacement. If, for example, the original average crustal density was ~2875 kg/m^3 (the average crustal density in the Great Valley Model 3 of *Godfrey and Klemperer* [1998]) and was later replaced by an average crustal density of 2750 kg/m^3 (the

average density of line 2, Figure 7), crustal thinning from 33 to 23 km could be accomplished without subsidence. Thermal expansion of the hot mantle could add an ephemeral uplift. The hypothesized crustal thickness in Plate 4b is therefore a maximum thickness. The present crustal thickness (19–23 km) requires crustal thinning to have occurred at some time during extension (Plate 4). Crustal thickness of the ICB is likely thinner by ~10 km from the original crustal thickness, considering that the ICB probably rifted within the forearc sequence (Figures 3 and 9), whose thickness onshore [*Ryberg and Fuis*, 1998] and under the Great Valley [*Godfrey and Klemperer*, 1998] is 30–35 km. Moreover, modeling indicates that for most crustal compositions a metamorphic core complex mode of extension typically takes place in continental crust whose thickness is >30–35 km [*Buck*, 1991].

Crouch and Suppe [1993] synthesized geological data to infer the origin of the ICB as a metamorphic core complex, based on exhumation of the Catalina Schist from midcrustal levels, widespread erosion along the rims of the ICB, and voluminous volcanism. In particular, Crouch and Suppe and *Bohannon and Geist* [1998] interpreted seismic reflection data nearshore as suggesting detachment faults and overlying remnants of fragmented and rifted hanging wall rocks. Our seismic reflection profiles (Figures 5a and 5b) located north of their profiles do not show clear evidence for detachment faults merging into the basement. The combined refraction and reflection data also show basin and ridge geometry with bounding faults, some of which extend to a depth of 8–10 km (Plates 1a and 1b).

Our observations do not necessarily contradict the interpretation of the ICB as a metamorphic core complex. Rather, they may indicate that extension continued in a different mode. Using thermomechanical models to model extension of the continental lithosphere, *Buck* [1991] pointed out that assuming constant heat flow throughout the extension phase, a metamorphic core complex mode of extension of a thick crust will eventually change to a wide rift extensional mode. Continued crustal thinning could lead to narrow rifting and ultimately to the formation of a mid-ocean ridge. We suggest that extension in the ICB in the vicinity of our seismic profiles started as a metamorphic core complex but proceeded as a wide rift (Basin and Range) mode, because there is no clear rift structure within the ICB north of San Diego. From San Diego Trough farther south, the Borderland may have started extending or continued to extend in a narrow rift mode, possibly even forming small spreading centers (Figure 1).

Plate 4 summarizes the evolution of the ICB as a forearc region subjected to slow subduction of young oceanic microplates. The termination of subduction was followed by rotation and northward translation of the Transverse Ranges starting between 20 and 18 Ma, which are attributed to the capture of the stalled Monterey microplate by the Pacific Plate [*Nicholson et al.*, 1994]. The resultant rapid extension and a possible tear in the underlying Monterey microplate provided the thermomechanical conditions for metamorphic core complex mode of extension, voluminous volcanism, and rapid isostatic uplift (Plate 4b). Continued extension probably took place as a wide rift mode similar to the Basin and Range. This resulted in crustal thinning and subsidence of the area, possibly to its present average depth (Plate 4c). A change in relative plate motion and inboard migration of the Pacific-North American Plate boundary terminated the extension and possibly caused a reversal of motion on some of the faults (Plate 4d).

7.2. Magmatism and Uplift

The volume and composition of volcanic rocks around the ICB are in agreement with continental extension in the presence of high subcrustal temperatures. Thick (>500 m) volcanic sections are exposed or drilled around the ICB [*Crouch and Suppe*, 1993; *Weigand and Savage*, 1993]. Their composition varies from tholeitic to calc-alkaline. Petrogenesis of these volcanic rocks and trace element composition indicate that they were derived by an interaction of a very young depleted oceanic lithosphere with the continental margin [*Weigand and Savage*, 1993; *Cole and Basu*, 1995]. The rocks have low $^{87}Sr/^{86}Sr$ ratios (<0.7040) and low $\delta^{18}O$, suggesting that they were derived partly from a mantle source [*Johnson and O'Neil*, 1984]. Extension of the subforearc lithosphere probably led to some decompression melting of mantle peridotite. Our hypothetical geothermal gradient discussed in section 7.3 (Figure 9a) also suggests temperatures in excess of the solidi of dry red clay, dry basalt, and amphibolite, implying partial melting of the lower part of the forearc (including ophiolites) and of the fossil ocean crust during and shortly after extension.

A localized heat source, such as a linear zone of mantle upwelling, was suggested to be an essential driving force for the formation of metamorphic core complexes off Papua New Guinea, where a spreading center is propagating into the continental lithosphere [*Hill et al.*, 1995]. The heat source for the ICB is hypothesized to be a "slab gap" due to the tearing of the underlying stalled young Monterey microplate when the North American Plate was captured by the Pacific Plate (Figure 3). The temporal relationship between magmatism and the uplift of the ICB may indicate, however, that in some places, mantle upwelling was a product of the extension, rather than the driving force for the formation of core complexes. The San Onofre Breccia is the erosional product derived from already uplifted blocks of Catalina Schist. On the basis of field relationships to volcanic and sedimentary formations it is dated as Early Miocene (~20–18 Ma) in the Channel Islands and as mid-Miocene (~17–14 Ma) in age between Los Angeles and San Diego and around Pt. Dume on the Malibu coast [*Stuart*, 1979]. Igneous rocks at numerous sites in the Borderland and coastal California mostly range between 17 and 13 Ma [*Weigand*, 1994; *Weigand and Savage*, 1993], i.e., later than the erosional products in the Channel Islands and concurrent with or slightly later than those in other places.

7.3. Thermomechanical Structure

Thermomechanical models suggest that metamorphic core complexes are formed during continental extension only in the presence of very high subcrustal temperatures which permit crustal-scale ductile flow [*Buck*, 1991]. Heat flow values in the California Borderland and coastal southern California are unusually high for a continental crust (70–100 mW/m^2) and are compatible with an extension event 19–13 Myr ago. Phase relationships and the crystallization order of melting products in the lower member of the Conejo volcanic rocks suggest that the melt source was at a temperature of ~1200°C and pressure of 7.5 kbar (~22.5 km depth) [*Hurst*, 1982]. Figure 9 presents a thermal model for the ICB, which follows the evolutionary scenario suggested in Plate 4. We assume the region to be a 33-km-thick forearc crust underlain by a young (~4 Ma) subducted microplate which was stalled for ~1 Myr prior to extension. Lithospheric thickness (to a depth of 1250°C) at this stage is estimated to be 55 km, and the surface is assumed to be close to sea level. At 19 Ma (time 0) the mantle lithosphere

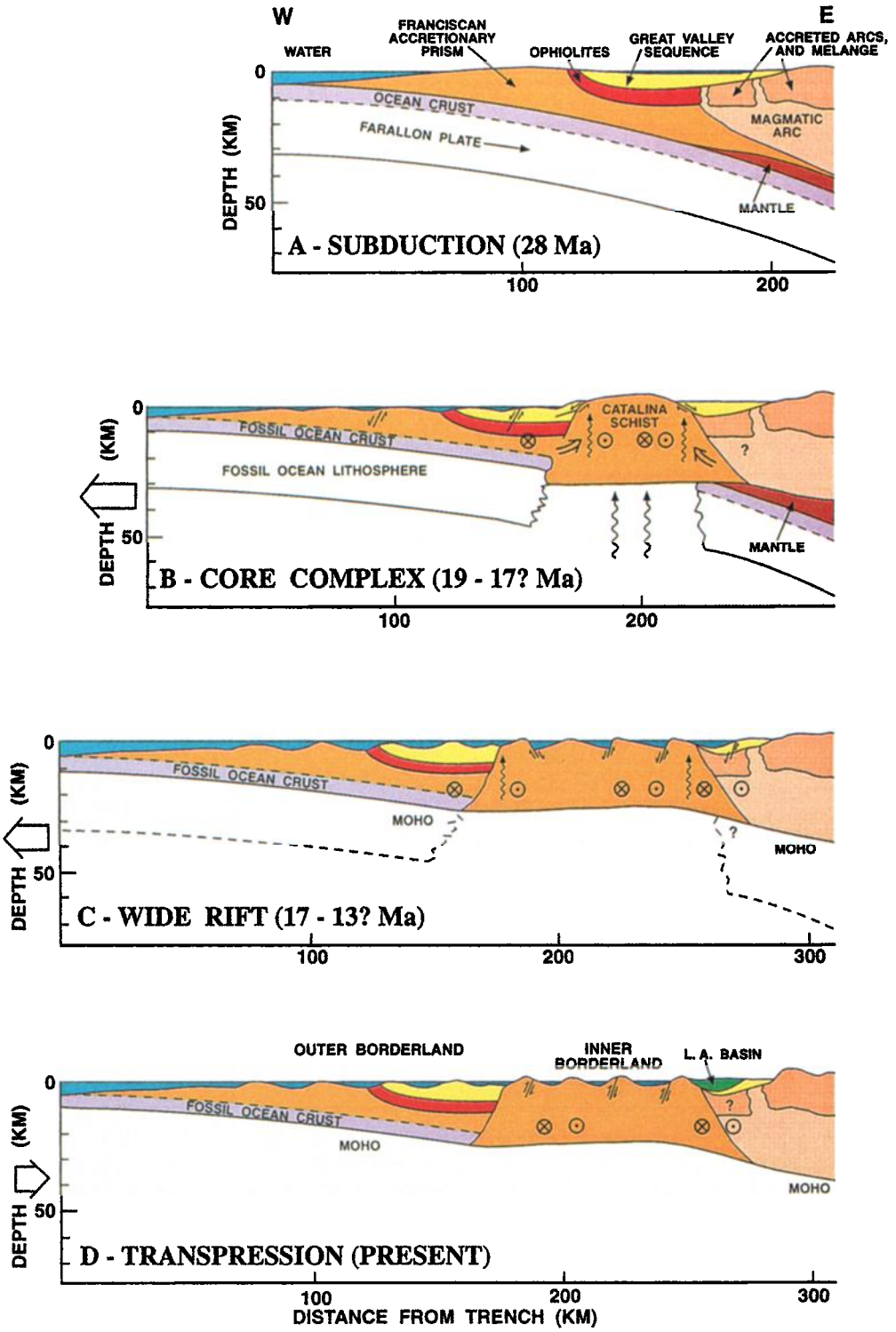

Plate 4. Schematic cross section showing tectonic development of the southern California margin. (a) At the end of subduction (modified from *Crouch and Suppe* [1993]). (b) Crustal extension in the form of a metamorphic core complex and partial melt rising through a gap in the fossil oceanic lithosphere. Franciscan-type metamorphic rocks underlying part of the subduction complex flowed into the extending area to form a crust made entirely of Catalina Schist. Extension was accompanied by an ephemeral uplift. Northward translation of the Outer Continental Borderland relative to the Inner Continental Borderland and internal strike-slip motion within the Inner Continental Borderland are represented by arrow tips and tails. (c) Probable continuation of extension in the form of high-angle normal faults in the upper crust [e.g., *Bohannon and Geist*, 1998], resulting in crustal thinning and basin and ridge topography. (d) Present schematic cross section of the California Borderland.

is thinned by an instantaneous extension bringing asthenospheric temperatures (1250°C) to a depth of 33 km. The crust is progressively thinned for an additional 6 Myr to a thickness of 22 km, as the 1250°C isotherm continues to track the base of the forearc crust. Upon cessation of extension, the model is allowed to return to thermal equilibrium. The imposed extension brings the surface heat flow to ~135 mW/m^2 and lower crustal temperatures to near solidus of the forearc and the fossil oceanic crust (Figure 9), and these conditions allow rapid lower crustal flow [e.g., *Buck*, 1991]. They also allow magma generation within the lower crust, and the former subducted plate, as discussed in section 7.2. Advection, which was not considered here, will speed the heating process. Surface heat flow at present (i.e., 19 Myr after extension) is also predicted to be unusually high (Figure 9b), in accord with observations [*Lee and Henyey*, 1975].

Uplift is predicted to occur during the first 4 Myr of extension (Figure 9b) when subsidence due to crustal thinning is not sufficiently large to counteract uplift due to thermal expansion. This result is compatible with the observations discussed in section 7.2 of uplift during the early part of the extensional and magmatic activity. The magnitude of uplift and subsidence depends on the possibility of crustal density change during extension due to compositional changes during core complex formation, crustal flow, and erosion. We chose a small average density reduction from 2830 to 2750 kg/m^3 to reach the present depth of 1300 m, a depth close to that observed in the Catalina Basin. This density reduction is small relative to that predicted from comparing gravity models of the Great Valley [*Godfrey and Klemperer*, 1998] with those of Figure 7.

The distribution of heat flow across the margin has a maximum located at the ICB and an increase southward along the ICB [*Lee and Henyey*, 1975]. This distribution is suggestive of the location of maximum extension at the ICB and the southward migration of extension through time, both of which are compatible with the tectonic model for this area (Figure 3; *Nicholson et al.* [1994]). The thermal regime of the Los Angeles Basin was also likely affected by the extension of the ICB. Previous subsidence models which considered the Los Angeles Basin as an isolated narrow (25 km wide) zone of later extension (12 Ma) on a cold lithosphere predict geothermal gradient of only 25°C/km [*Sawyer et al.*, 1987]. However, the average value of geothermal gradients measured to depths >4 km in the Los Angeles Basin is 39.1°C/km [*Jeffrey et al.*, 1991]. Using a porosity-dependent conductivity range of 1.6–2.07 W m^{-1}°C^{-1} for depths between 1 and 4 km [*Sawyer et al.*, 1987], the heat flow by this gradient is between 63 and 81 mW/m^2, which is within the range predicted by our model. Hence the thermal signature of the Los Angeles Basin may be at least in part due to the more regional event of ICB extension.

8. Summary

The seismic structure of the ICB crust is characterized by the following observations: (1) localized pockets, <2 km thick, of low-velocity sediments, (2) relatively high upper crustal velocity averaging 5.7 and 5.6 km/s for lines 1 and 2, respectively, (3) homogenous P wave velocity averaging 6.3 and 6.5 km/s for lines 1 and 2, respectively, for the crust below 8 km depth, (4) relatively flat Moho at 19–20 and 22–23 km depth for these lines, respectively, (5) weak fine-scale reflectivity between 4 and 7 s two-way travel time under Catalina Ridge, and (6) no indication for a high-velocity layer at the base of the crust.

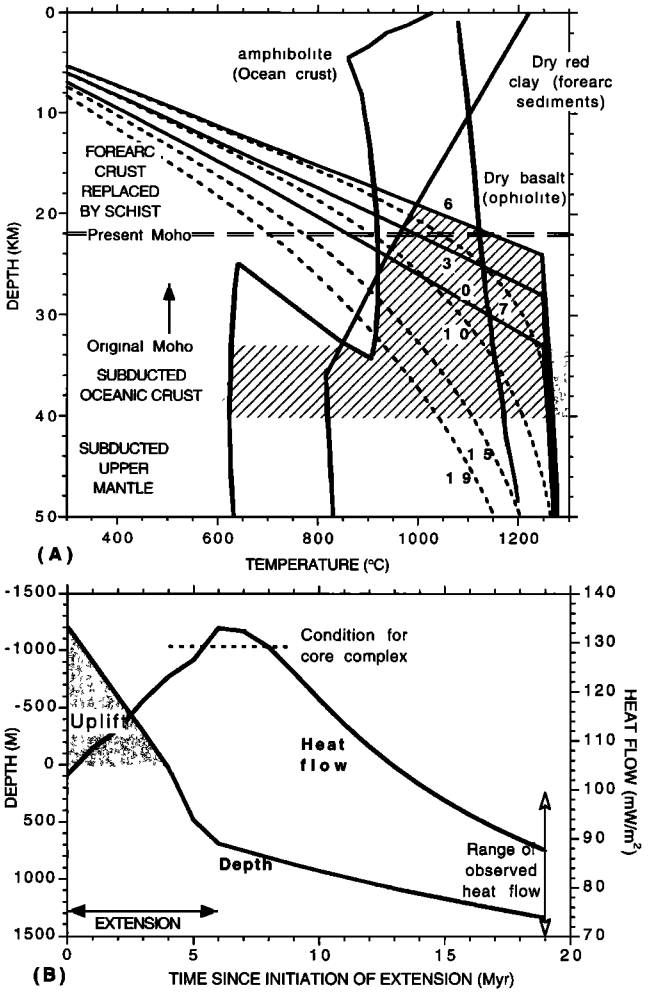

Figure 9. A thermal model following the forearc extension scenario of Plates 4a–4c. (a) Calculated geothermal gradients for different times (in Myr) after extension started. (b) Heat flow and surface uplift. Prior to extension, we assume a young (4 Ma), recently (for 1 Myr) stalled subducted slab underlying a 33-km-thick forearc whose surface is near sea level [*Dumitru*, 1991]. At 19 Ma (time 0) the mantle lithosphere is thinned by an instantaneous extension bringing asthenospheric temperatures (1250°C) to a depth of 33 km. The 1250°C isotherm continues to rise gradually during the next 6 Myr to a final depth of 22 km. Upon cessation of extension, the model is allowed to return to thermal equilibrium. The evolving geothermal gradients with time were calculated using a finite difference scheme with vertical grid of 0.5 km to depth of 125 km; time step of 8000 years; bottom and surface temperatures of 1350°C and 20°C, respectively; specific heat of 1 J kg^{-1} °C^{-1}; crust and mantle thermal conductivities of 2.5 and 3.3 W m^{-1}°C^{-1}, respectively; and an exponential radiogenic heat production within the forearc with a "skin depth" of 10 km and a surface production rate of 1.25 μWm^{-3}. Horizontal conduction was neglected. Also plotted are solidi for amphibolite [*Wyllie and Wolf*, 1993], dry red clay [*Nichols et al.*, 1996], and dry basalt [*Peacock*, 1996]. Partial melt is expected during and shortly after extension (hatched regions) at depths where the temperature is higher than the solidi. Figure 9b shows calculated heat flow, uplift, and subsidence from the above model. Uplift/subsidence is calculated relative to the lithosphere prior to extension. Double-headed arrow, range of observed heat flow [*Lee and Henyey*, 1975]; dashed line, surface heat flow necessary for a metamorphic core complex mode of extension [*Buck*, 1991].

Observations 4 and 6 rest on our interpretation of a dominant reflection between 45 and 160 km offset in the wide-angle data as *PmP*. The seismic and gravity data also delineate the boundaries of the ICB with mainland California and with the OCB. The boundary with mainland California is characterized by crustal thickening from the shelf edge inland. The boundary with the OCB is characterized by an increasing Bouguer gravity anomaly over the OCB and by change in the seismic stratigraphy.

Compared with the seismic velocity structure of the fossil accretionary prism and forearc regions of the California subduction system, the ICB has lost its overlying lower velocity sediments and crustal layers and its basal high-velocity part. The near absence of sediments, despite the location of the ICB in the former forearc, probably indicates erosion of the upper crustal section. This is in agreement with the suggestion that Catalina Schist was exhumed from depths of 10–15 km during the Miocene [*Crouch and Suppe*, 1993] and with other geological evidence for subaerial exposure of the ICB during that time. The observed crustal seismic velocities are similar to laboratory-measured *P* wave velocity of metamorphic rocks of Franciscan origin, the Pelona Schist, except for the lowermost crust, which has a slightly higher average velocity [*McCaffree-Pellerin and Christensen*, 1998; N. Christensen, personal communication, 1999]. We therefore interpret the crustal velocity structure to indicate a crust made almost uniformly of Catalina Schist. The crustal velocity structure is compatible with the suggestion of a regional-scale crustal flow [*Block and Royden*, 1990] into the ICB during extension in the form of metamorphic core complexes [*Crouch and Suppe*, 1993]. It is incompatible with the suggestion of adding large volumes of mantle-derived material to the base of the crust during extension [*Gans*, 1989; *Hill et al.*, 1995]. However, contrary to previous interpretations of seismic reflection lines [*Crouch and Suppe*, 1993; *Bohannon and Geist*, 1998], our seismic reflection profiles do not show clear evidence for low-angle detachment faults merging into the basement. Moreover, our combined refraction and reflection data show basin and ridge geometry with high-angle bounding faults, some of which extend to a depth of 8–10 km. To reconcile the various observations, we suggest that extension in the ICB in the vicinity of our seismic profiles may have started as a metamorphic core complex but proceeded as a wide rift (Basin and Range style). Uplift of the surface of the ICB could have been caused by thermal expansion and by the replacement of the original crustal column by a thinner column having a lower average crustal density.

The tectonic event causing this extension may have been the capture of the stalled Monterey microplate and the overlying North American margin by the Pacific Plate [*Nicholson et al.*, 1994]. The capture resulted in the rotation of the western Transverse Ranges and possibly in a tear or a gap in the underlying Monterey microplate, which encouraged short-lived mantle upwelling. The volume and composition of volcanic rocks around the ICB are in agreement with continental extension in the presence of high subcrustal temperatures. Heat flow values in the California Borderland and coastal southern California are also unusually high for the continental crust (70–100 mW/m^2), and their geographical distribution is compatible with an extension event in the ICB during the Early and Middle Miocene. Among the likely effects of the ICB's tectonic history are the thermal regime of the Los Angeles Basin and the shallow depths of earthquake epicenters offshore Los Angeles [*Magistrale and Zhou*, 1996].

Appendix: Uncertainty of the Tomographic Solution

A1. Qualitative Approach

The root-mean-square (RMS) misfit between the calculated and observed travel time curves is 140 ms (*Zhang et al.*, 1998, Figure 8). In particular, the gradient or the shape of the calculated arrival matches the observed curve well. A smaller RMS fit can be achieved at the expense of making the model velocity less smooth. Comparison of the uppermost model velocity with coincident MCS reflection profiles shows that low-velocity pockets in the model just below the seafloor correspond to small sedimentary basins imaged by the MCS data, most notably the folded sedimentary section in San Pedro Basin on line 1 (Plate 1a). This fit was achieved despite the fact that the initial model included a uniform velocity below the seafloor and indicates that the horizontal resolution is better than 4 km in the upper part of the model. The lack of fit on the northern end of line 1 where the sediments on the MCS profile thicken landward is caused by poor ray coverage.

A2. Quantitative Approach

A covariance matrix was calculated between many models, which are generated with random slowness errors (Monte Carlo simulations), and the original model. The random errors in the average and apparent slowness are due to uncertainties in picking individual points, in the first break of the entire arrival, and in the gradient of the arrival travel time. The diagonal elements of the covariance matrix represent the uncertainties of the model parameters. To find how well the velocity at each point is resolved, the correlation between the uncertainty of each model parameter and the uncertainty of all other model parameters is calculated [*Zhang et al.*, 1998]. Ideally, the uncertainty of any point in the model should be independent of the rest of the model. However, if the correlation with other parts of the model is highly positive or highly negative, the parameters have not been independently resolved and represent a linear combination with other values.

For line 1 we selected a point at a depth of 5 km under the high-velocity structure under Catalina Island where the velocity structure varies laterally over a short distance (Plate 2a). For line 2 the point selected for uncertainty analysis is located at a depth of 7 km under the high-velocity structure under San Clemente Fault (Plate 2b). Both points are covered by diving waves, and the point on line 2 is covered to a lesser extent by reflections. To minimize computation, the uncertainty analysis was done only for the refraction (diving waves) arrivals. Plate 5 shows a high (>0.5) correlation only in a small area, 5 km × 3 km for line 1 and 8 km × 3 km for line 2. In addition, a 6-km-wide region to the south of the selected point on line 1 is negatively correlated (less than −0.5) with that point. Hence the depth resolution due to imaging by diving waves is high even in areas of complex topography and subsurface structure, but the horizontal resolution is smeared over several kilometers. This smearing is due to the fact that diving waves mainly travel horizontally through the medium, and therefore travel time perturbations can be distributed anywhere along their paths.

The lateral resolution in the upper part of the crust is, in fact, better than shown by the Monte Carlo simulations, because this area is also sampled by Moho reflections which propagate subvertically (Plates 2a and 2b). These arrivals are sensitive to horizontal perturbations but are much less sensi-

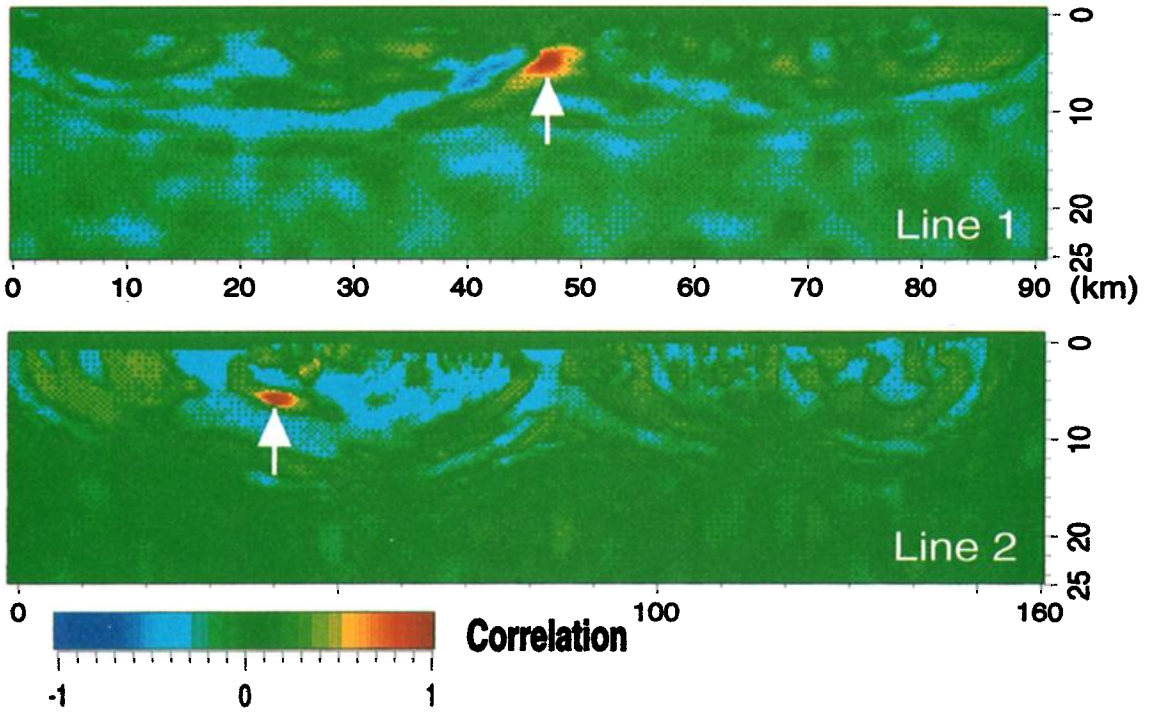

Plate 5. Posterior model correlation using nonlinear Monte Carlo simulations for points (marked with arrows) under Catalina Ridge (line 1) and under San Clemente Ridge (line 2).

tive to variations with depth. Because the velocity below depths of 8–10 km is resolved solely by fitting wide-angle reflections from the Moho (*PmP*), variations of velocity with depth are less well constrained.

Acknowledgments. We thank Southern California Marine Institute, Captain Jim Cvitanovich and the crew of the R/V *Yellowfin* for their work and hospitality during the cruise, Greg Miller, Dave Foster, and Robert Iuliucci for OBS operation, Dave Foster and Rebecca Drury for help with data processing, and Jeremy Loss, Philipp Molzer, and Jeff Zwinakis for help with the figures. Keith Louden, Dalhousie University, kindly loaned us three OBSs. The PASSCAL Instrument Facility kindly provided the Refteks used during LARSE. We thank Craig Nicholson, Mark Legg, and Tanya Atwater for illuminating discussions and Philipp Molzer and Ingo Pecher for useful comments. Helpful reviews by Associate Editor Walter Mooney and an anonymous referee are gratefully acknowledged. The LARSE experiment was funded by NSF EAR-9416774, the U.S. Geological Survey's Earthquake Hazards and Coastal and Marine Programs, and by the Southern California Earthquake Center (SCEC). SCEC is funded by NSF Cooperative Agreement EAR-8920136 and USGS Cooperative Agreements 14-08-0001-A0899 and 1434-HQ-97AG01718. Finite difference thermal conduction modeling was written and computed using the University of Southern California Geophysics computational facilities. SCEC contribution 486.

References

Atwater, T., Plate tectonic history of the northeast Pacific and western North America, in *The Eastern Pacific Ocean and Hawaii*, edited by E. L. Winterer, D. M. Hussong, and R. W. Decker, pp. 29–72, Geol. Soc. of Am., Boulder, Colo., 1989.

Atwater, T., and J. Severinghaus, Tectonic maps of the northeast Pacific, in *The Geology of North America*, vol. N, *The Eastern Pacific Ocean and Hawaii*, edited by E. L. Winterer, D. M. Hussong, and R. W. Decker, pp. 15–28, Geol. Soc. of Am., Boulder, Colo., 1989.

Atwater, T., and J. Stock, Pacific-North America plate tectonics of the Neogene southwestern United States: An update, *Int. Geol. Rev.*, *40*, 375–402, 1998.

Bennett, R. A., W. Rodi, and R. E. Reilinger, Global position system constraints on the fault slip rates in southern California and northern Baja, Mexico, *J. Geophys. Res.*, *101*, 21,943–21,960, 1996.

Bird, P., and R. W. Rosenstock, Kinematics of present crust and mantle flow in southern California, *Geol. Soc. Am. Bull.*, *95*, 946–957, 1984.

Block, L., and L. H. Royden, Core complex geometries and regional scale flow in the lower crust, *Tectonics*, *9*, 557–567, 1990.

Bohannon, R. G., and E. Geist, Upper crustal structure and Neogene tectonic development of the California Continental Borderland, *Geol. Soc. Am. Bull.*, *110*, 779–800, 1998.

Brocher, T. M., R. W. Clayton, K. D. Klitgord, R. G. Bohannon, R. Sliter, J. K. McRaney, J. V. Gardner, and J. B. Keene, Multichannel seismic reflection profiling on the R/V *Maurice Ewing* during the Los Angeles Region Seismic Experiment (LARSE), California, *U.S. Geol. Surv. Open File Rep.*, *95-228*, 73 pp., 1995.

Brocher, T. M., A. L. Ruebel, T. L. Wright, and D. A. Okaya, Compilation of 20 sonic and density logs from 12 oil test wells along LARSE Lines 1 and 2 in the Los Angeles Basin, California, *U.S. Geol. Surv. Open File Rep.*, *98-366*, 53 pp., 1998.

Brocher, T. M., U. S. ten Brink, and T. Abramovitz, Synthesis of crustal seismic structure argues against a slab gap beneath coastal California, *Int. Geol. Rev.*, *41*, 263–274, 1999.

Buck, W. R., Modes of continental lithospheric extension, *J. Geophys. Res.*, *96*, 20,161–20,178, 1991.

Christensen, N. I., and W. D. Mooney, Seismic velocity structure and composition of the continental crust: A global view, *J. Geophys. Res.*, *100*, 9761–9788, 1995.

Cole, R. B., and A. R. Basu, Nd-Sr isotopic geochemistry and tectonics of ridge subduction and middle Cenozoic volcanism in western California, *Geol. Soc. Am. Bull.*, *107*, 167–179, 1995.

Crandall, G. J., B. P. Luyendyk, M. S. Reichle, and W. A. Prothero, A marine seismic refraction study of the Santa Barbara Channel, California, *Mar. Geophys. Res.*, *5*, 15–37, 1983.

Crouch, J. K., and J. Suppe, Late Cenozoic tectonic evolution of the Los Angeles Basin and Inner California Borderland: A model for core complex-like crustal extension, *Geol. Soc. Am. Bull.*, *105*, 1415–1434, 1993.

Davis, T. L., and J. S. Namson, A balanced cross-section of the 1994 Northridge earthquake, southern California, *Nature*, *372*, 167–169, 1994.

Dickinson, W. R., Tectonic implications of Cenozoic volcanism in coastal California, *Geol. Soc. Am. Bull.*, *109*, 936–954, 1997.

Dumitru, T. A., Effects of subduction parameters on geothermal gradients of forearcs, with an application to Franciscan subduction in California, *J. Geophys. Res.*, *96*, 621–641, 1991.

Fuis, G. S., et al., Images of crust beneath southern California will aid study of earthquakes and their effects, *Eos Trans. AGU*, *77*, 173, 176, 1996.

Gans, P. B., G. A. Mahood, and E. R. Schermer, Synextensional magmatism in the Basin and Range Province: A case study from the eastern Great Basin, *Spec. Pap. Geol. Soc. Am.*, *233*, 53 pp., 1989.

Godfrey, N. J., and S. L. Klemperer, Ophiolitic basement to a forearc basin and implications for continental growth: The Coast Range/Great Valley ophiolite, California, *Tectonics*, *17*, 558–570, 1998.

Hamilton, E. L., Sound velocity-density relations in sea-floor sediments and rocks, *J. Acoust. Soc. Am.*, *63*, 366–377, 1978.

Harrison, J. C., R. E. von Huene, and C. E. Corbato, Bouguer gravity anomalies and magnetic anomalies off the coast of southern California, *J. Geophys. Res.*, *71*, 4921–4941, 1966.

Hauksson, E., and J. S. Haase, Three-dimensional Vp and Vp/Vs velocity models of the Los Angeles basin and central Transverse Ranges, California, *J. Geophys. Res.*, *102*, 5423–5453, 1997.

Hearn, T. M., and R. W. Clayton, Lateral velocity variations in southern California, II, Results for the lower crust from Pn waves, *Bull. Seismol. Soc. Am.*, *76*, 511–520, 1986.

Hill, E. J., S. L. Baldwin, and G. S. Lister, Magmatism as an essential driving force formation of active metamorphic core complexes in eastern Papua New Guinea, *J. Geophys. Res.*, *100*, 10,441–10,451, 1995.

Humphreys, E. D., and B. H. Hager, A kinematic model for the late Cenozoic development of southern California crust and upper mantle, *J. Geophys. Res.*, *95*, 19,747–19,762, 1990.

Hurst, R. W., Petrogenesis of the Conejo volcanic suite, southern California, *Geology*, *10*, 267–272, 1982.

Ingersoll, R. V., and P. E. Rumelhart, Three-stage evolution of the Los Angeles Basin, southern California, *Geology*, *27*, 593–596, 1999.

Jeffrey, A. W. A., H. M. Alimi, and P. D. Jenden, Geochemistry of Los Angeles Basin oil and gas systems, in *Active Margin Basins*, edited by K. T. Biddle, 197–219, *AAPG Mem.*, *50*, 1991.

Johnson, C. M., and J. R. O'Neil, Triple junction magmatism: A geochemical study of Neogene volcanic rocks in western California, *Earth Planet. Sci. Lett.*, *71*, 241–262, 1984.

Junger, A., and H. C. Wagner, Geology of the Santa Monica and the San Pedro basins, California Continental Borderland, *U.S. Geol. Surv. Misc. Field Stud. Map*, *MF-0820*, 5 sheets, 1977.

Kohler, M. D., and P. Davis, Crustal thickness variations in southern California from Los Angeles Region Seismic Experiment passive phase teleseismic travel time, *Bull. Seismol. Soc. Am.*, *87*, 1330–1344, 1997.

Langenheim, V. E., and R. C. Jachens, Gravity data collected during the Los Angeles Regional Seismic Experiment (LARSE) and preliminary model of regional density variations in basement rocks, Southern California, *U.S. Geol. Surv. Open File Rep.*, *96-682*, 25 pp., 1996.

Lee, T.-C., and T. L. Henyey, Heat flow through the southern California Borderland, *J. Geophys. Res.*, *80*, 3733–3743, 1975.

Luyendyk, B. P., A model for Neogene crustal rotations, transtension, and transpression in southern California, *Geol. Soc. Am. Bull.*, *103*, 1528–1536, 1991.

Magistrale, H., and H. Zhou, Lithologic control of the depth of earthquakes in southern California, *Science*, *273*, 639–642, 1996.

Mann, P., and M. B. Gordon, Tectonic uplift and exhumation of blueschist belts along transpressional strike-slip fault zones, in *Subduction: Top to Bottom, Geophys. Monogr. Ser.*, vol. 96, edited by G. E. Bebout et al., pp. 143–154, AGU, Washington, D. C., 1996.

McCaffree-Pellerin, C. L., and N. I. Christensen, Interpretation of crustal seismic velocities in the San Gabriel-Mojave region, southern California, *Tectonophysics*, *286*, 253–271, 1998.

McCarthy, J., S. P. Larkin, G. S. Fuis, R. W. Simpson, and K. A. Howard, Anatomy of a metamorphic core complex: Seismic refraction/wide-angle reflection profiling in southeastern California and western Arizona, *J. Geophys. Res.*, *96*, 12,259–12,291, 1991.

Miller, K. C., J. M. Howie, and S. D. Ruppert, Shortening within underplated oceanic crust beneath the central California margin, *J. Geophys. Res.*, *97*, 19,961–19,980, 1992.

Miller, K. C., M. Dober, F. Hua, and R. G. Bohannon, Crustal gravity models along seismic reflection profiles, California Continental Borderland, *Eos Trans. AGU*, *77*(46), Fall Meet. Suppl., F737, 1996.

Moser, T. J., Shortest ray path calculation of seismic rays, *Geophysics*, *56*, 59–67, 1991.

Nichols, G. T., P. J. Wyllie, and C. R. Stern, Experimental melting of pelagic sediment, constraints relevant to subduction, in *Subduction: Top to Bottom, Geophys. Monogr. Ser.*, vol. 96, edited by G. E. Bebout et al., pp. 293–298, AGU, Washington, D. C., 1996.

Nicholson, C., C. C. Sorlien, T. Atwater, J. C. Crowell, and B. P. Luyendyk, Microplate capture, rotation of the western Transverse Ranges, and initiation of the San Andreas transform as a low-angle fault system, *Geology*, *22*, 491–495, 1994.

Okaya, D. A., J. Bhowmic, G. S. Fuis, J. M. Murphy, M. C. Robertson, A. Chakraborty, M. L. Benthien, K. Hafner, and J. J. Norris, Report for air-gun data acquired at onshore stations during the 1994 Los Angeles Region Seismic Experiment (LARSE), California, *U.S. Geol. Surv. Open File Rep.*, *96-297*, 224 pp., 1996.

Peacock, S., Thermal and petrologic structure of subduction zones, in *Subduction: Top to Bottom, Geophys. Monogr. Ser.*, vol. 96, edited by G. E. Bebout et al., pp. 119–133, AGU, Washington, D. C., 1996.

Ryberg, T., and G. S. Fuis, The San Gabriel Mountains reflective zone: Possible evidence for mid-crustal thrust faulting, *Tectonophysics*, *286*, 31–46, 1998.

Sawyer, D. S., A. T. Hsui, and M. N. Toksoz, Extension, subsidence and thermal evolution of the Los Angeles Basin: A two-dimensional model, *Tectonophysics*, *133*, 15–32, 1987.

Shaw, J. H., and J. Suppe, Active faulting and growth folding in the eastern Santa Barbara Channel, California, *Geol. Soc. Am. Bull.*, *106*, 607–626, 1994.

Shaw, J. H., and J. Suppe, Earthquake hazards of active blind-thrust faults under the central Los Angeles Basin, California, *J. Geophys. Res.*, *101*, 8623–8642, 1996.

Shor, G. G., and R. W. Raitt, Seismic studies in the southern California Continental Borderland, paper presented at International Geological Congress, Section 9, Mexico, D. F., 1958.

Snyder, D. B., C. W. Roberts, R. W. Saltus, and R. F. Sikora, Description of magnetic tape containing the principal facts of 64,026 gravity stations in the state of California, *PB 82-168287*, magnetic tape and 34 pp., Natl. Tech. Inf. Serv., U.S. Dep. of Commer., Springfield, Ill., 1982.

Stadum, C. J., Fossil wood in a 13.5 Ma tuff breccia of the Conejo volcanics, Santa Monica Mountains, California, *AAPG Bull.*, *82*, 859, 1998.

Sung, L., and D. D. Jackson, Crustal and uppermost mantle structure under southern California, *Bull. Seismol. Soc. Am.*, *82*, 934–961, 1992.

Stuart, C. J., Middle Eocene paleogeography of coastal southern California and the California Borderland: Evidence from schist-bearing sedimentary rocks, in *Cenozoic Paleogeography of the Western United States*, edited by J. M. Armentrout, M. R. Cole, and H. TerBest Jr., pp. 29–44, Soc. for Sediment. Geol., Tulsa, Okla., 1979.

ten Brink, U. S., R. M. Drury, G. K. Miller, T. M. Brocher, and D. Okaya, Los Angeles Region Seismic Experiment (LARSE), California: Off-shore seismic refraction data, *U.S. Geol. Surv. Open File Rep.*, *96-27*, 1–29, 1996.

Vedder, J. G., Regional geology and petroleum potential of the southern California Borderland, in *Geology and Resource Potential of the Continental Margin of Western North America and Adjacent Ocean Basins: Beaufort Sea to Baja California*, edited by D. W. Scholl, A. Grantz, and J. G. Vedder, pp. 403–447, Circum-Pac. Counc. for Energy and Miner. Resour., Houston, Tex., 1987.

Ward, S. N., and G. Valensise, Progressive growth of San Clemente Island, California, by blind thrust faulting: Implications for fault slip partitioning in the California Continental Borderland, *Geophys. J. Int.*, *126*, 712–734, 1996.

Weigand, P. W., Timing and cause of Middle Tertiary magmatism in onshore and offshore southern California, *AAPG Bull.*, *78*, 676, 1994.

Weigand, P. W., and K. L. Savage, Review of the petrology and geochemistry of the Miocene Conejo volcanics of the Santa Monica Mountains, California, in *Depositional and Volcanic Environments of Middle Tertiary Rocks in Santa Monica Mountains, Southern California*, edited by P. W. Weigand, A. E. Fritsche, and G. E. Davis, vol. 72, pp. 93–112, Soc. for Sediment. Geol., Pac. Sect., Tulsa, Okla., 1993.

Wright, T., Structural geology and tectonic evolution of the Los Angeles basin, California, in *Active Margin Basins*, edited by K. T. Biddle, 35–134, *AAPG Mem.*, *50*, 1991.

Wyllie, P. J., and M. B. Wolf, Amphibolite dehydration-melting: sorting out the solidus, in *Magmatic Processes and Plate Tectonics*, edited by H. M. Prichard, T. Alabaster, N. B. Harris, and C. R. Neary, *Geol. Soc. Spec. Publ.*, *76*, 405–416, 1993.

Zelt, C. A., and R. B. Smith, Seismic traveltime inversion for 2-D crustal velocity structure, *Geophys. J. Int.*, *108*, 16–34, 1992.

Zhang, J., and M. N. Toksoz, Nonlinear refraction travel time tomography, *Geophysics*, *63*, 1726–1737, 1998.

Zhang, J., U. S. ten Brink, and M. N. Toksoz, Nonlinear refraction and reflection travel time tomography, *J. Geophys. Res.*, *103*, 29,743–29,758, 1998.

T. M. Brocher and G. S. Fuis, U.S. Geological Survey, 345 Middlefield Road, Mail Stop 977, Menlo Park, CA 94025. (brocher@andreas.wr.usgs.gov; fuis@andreas.wr.usgs.gov)

K. D. Klitgord, Exxon Exploration Co., P.O. Box 4778, Houston, TX 77210. (kim.d.klitgord@exxon.sprint.com)

D. A. Okaya, University of Southern California, Department of Geological Sciences, Los Angeles, CA 90089. (okaya@terra.usc.edu)

U. S. ten Brink, U.S. Geological Survey, Woods Hole Field Center, Quissett Campus, Woods Hole, MA 02543. (utenbrink@nobska.er.usgs.gov)

J. Zhang, Geotomo Ltd., 225 South Boulder Road, Suite 201, Louisville, CO 80027. (jie@geotomo.com)

(Received December 3, 1998; revised August 3, 1999; accepted September 8, 1999.)